CivilEng

MDPI

Article

Electro-Mechanical Impedance-Based Structural Health Monitoring of Fiber-Reinforced Concrete Specimens under Four-Point Repeated Loading

Maria C. Naoum [1], Constantin E. Chalioris [1,*], Chris G. Karayannis [2], Athanasios I. Karabinis [1] and Anaxagoras Elenas [1]

[1] Department of Civil Engineering, Democritus University of Thrace, 67100 Xanthi, Greece; mnaoum@civil.duth.gr (M.C.N.); karabin@civil.duth.gr (A.I.K.); elenas@civil.duth.gr (A.E.)
[2] Department of Civil Engineering, Aristotle University of Thessaloniki, 54124 Thessaloniki, Greece; karayannis@civil.auth.gr
* Correspondence: chaliori@civil.duth.gr

Abstract: Fiber Reinforced Concrete (FRC) has shown significant promise in enhancing the safety and reliability of civil infrastructures. Structural Health Monitoring (SHM) has recently become essential due to the increasing demand for the safety and sustainability of civil infrastructures. Thus, SHM provides critical benefits for future research to develop more advanced monitoring systems that effectively detect and diagnose the damage in FRC structures. This study investigates the potential of an Electro-Mechanical Impedance (EMI) based SHM system for detecting cracks in FRC prisms subjected to four-point repeated loading. For the needs of this research, an experimental investigation of three FRC specimens with the dimensions 150 × 150 × 450 (mm) were subjected to three different loading levels where no visual cracks formed on their surface. Next, prisms were subjected to reloading until they depleted their load-carrying capacity, resulting in pure bending fracture at the mid-span. A network of nine cement paste coated Piezoelectric lead Zirconate Titanate (PZT) transducers have been epoxy bonded to the surface of the FRC prisms, and their frequency signal measurements were utilized for quantitative damage assessment. The observed changes in the frequency response of each PZT sensor are evaluated as solid indications of potential damage presence, and the increasing trend connotes the severity of the damage. The well-known conventional static metric of the Root Mean Square Deviation (RMSD) was successfully used to quantify and evaluate the cracking in FRC specimens while improving the efficiency and accuracy of damage detection. Similarly, the dynamic metric of a new statistical index called "moving Root Mean Square Deviation" (mRMSD) was satisfactorily used and compared to achieve and enhance accuracy in the damage evaluation process.

Keywords: structural health monitoring (SHM); reinforced concrete (RC); fiber reinforced concrete (FRC); piezoelectric lead zirconate titanate (PZT); real-time structural monitoring; damage diagnosis

check for updates

Citation: Naoum, M.C.; Chalioris, C.E.; Karayannis, C.G.; Karabinis, A.I.; Elenas, A. Electro-Mechanical Impedance-Based Structural Health Monitoring of Fiber-Reinforced Concrete Specimens under Four-Point Repeated Loading. *CivilEng* **2023**, *4*, 856–880. https://doi.org/10.3390/civileng4030047

Academic Editors: Akanshu Sharma and Angelo Luongo

Received: 2 June 2023
Revised: 6 July 2023
Accepted: 12 July 2023
Published: 31 July 2023

1. Introduction

Fiber Reinforced Concrete (FRC) is a composite material of concrete and steel, glass, or synthetic fibers used to increase and improve its mechanical properties. Recently, FRC has gained significant attention in structural engineering applications thanks to its improved concrete structures' strength, ductility, and durability. Thus, FRC is widely used in infrastructure construction and civil engineering projects such as large-scale buildings, bridges, road networks, ports, railways, and tunnels [1]. However, although there are many advantages to using FRCs in infrastructure construction, these structures are still vulnerable to damage and deterioration caused by various factors, such as environmental conditions, exposure to high temperatures, freeze–thaw cycles, aging, and repeated loading [2].

Incorporating fibers into concrete enhances its strength, toughness, resistance to cracking, and ability to withstand tension. The fibers, which are randomly dispersed throughout the material, effectively restrict the unsteady spread of cracks at both micro and macro scales [3]. Furthermore, various research works have shown that fibers greatly influence crack propagation [4] and control, as FRC exhibits stress-softening behavior even after the appearance of macrocracks [5]. In particular, using environmentally friendly materials for manufacturing fibers that will be used in producing FRC has recently opened new avenues for research [6]. Synthetic fibers also contribute to a diminished environmental impact, aligning with the goals of sustainable construction and circular economies [7]. Additionally, using short synthetic fibers as reinforcement for concrete has been thoroughly investigated in many research works [8].

However, recent experimental studies have shown that their low modulus of elasticity limits their ability to transfer stress between tension cracks, and non-metallic fibers seem to contribute less to FRC's post-cracking behavior than to other steel fibers [9]. Also, some studies have reported a slight improvement in direct and indirect tensile strength, such as splitting and bending tests using synthetic fibers [10]. Further, existing studies have indicated that polypropylene macro synthetic FRC exhibits improved post-cracking characteristics, particularly ductility and tensile behavior [11,12]. This type of synthetic fiber reduces the opening and limits the propagation of microcracks, as a result of which the fiber concrete performs improved tensile and compressive strength [13].

Real-time Structural Health Monitoring (SHM) is the process of continuously monitoring and evaluating the structural integrity of a building or infrastructure in real-time using various sensors and methods. SHM has recently emerged as an essential research topic in civil engineering due to the increasing demand for the safety and sustainability of civil infrastructures. Thus, effective techniques can be developed to assess structures' condition and detect potential damage before it leads to catastrophic failure. A promising approach of SHM is the application of Electro-Mechanical Impedance (EMI) through the ability of Piezoelectric lead Zirconate Titanate (PZT) transducers to acquire information about the structural integrity of the examined member.

Early detection of failures in critical structural members of reinforced concrete structures is crucial to prevent further structural degradation, and sudden collapses due to brittle shear failures lead to significant economic and social impacts [14]. A practical approach to address this issue is to transact continuous, real-time in situ monitoring to detect damages and promptly evaluate the degree of severity [15,16]. The application of SHM in FRC is of great interest because of the enhanced ductility of FRC and the ability of PZTs to detect even small changes in structural behavior, such as cracks or deformation [17].

Furthermore, the utilization of small-sized piezoelectric transducers that could be surface-bonded or embedded has gained widespread acceptance in EMI-based methods for SHM of concrete structural members due to their ability to act as both (a) a sensor, receiving a mechanical signal, and (b) an actuator, creating a mechanical vibration [18,19]. A reliable assessment methodology was successfully developed for SHM and assessing damage identification levels in RC structural members through a thorough investigation by Chalioris et al. [20]. Notably, the reinforced concrete structural members were subjected to monotonic [21] or cyclic loading [22]. At the same time, real-time measurements from a network of PZT transducers installed in critical regions of the structural members were carried out. The abovementioned methodology was deemed effective even in SHM and damage diagnosis of real-scale specimens such as RC frames or beam–column joint sub-assemblages [23].

As can be seen from the previous references, the novelty of the present study is focused on the following issues: (a) The randomness of the fibers in the mass of cement-based materials and the complexity of fibrous matrices limit the number of existing studies on the SHM techniques to localize damage due to cracking in FRC [24]; (b) there are several ways to coat and protect the PZT patches mounted to the structural member, such as covering with silicon, epoxy resin, etc. However, in these cases, the transducers are not replaceable after structural damage or due to malfunctioning situations, and there is no relevant research on the configuration control of reusable PZTs. A network of novel patches that have been coated with cement paste and then epoxy bonded to the surface of the FRC specimens are used to provide a solution of durable and replaceable PZTs. (c) Real-time early diagnosis of FRC structural damages caused by fatigue or repetitive/seismic loading is a complex and time-consuming process due to the large number of measurements and transducers needed [25]. Four-point bending tests of FRC prismatic specimens under a repetitive load simulating these conditions are performed to fulfill these challenges. This research adopts and experimentally investigates a new, efficient, easy-to-apply, and feasible integrated SHM procedure.

The experimental program of this study includes three specimens to evaluate the effectiveness of an interesting SHM approach using an EMI-based, custom-made SHM device and a network of PZT transducers attached to the surface of the prisms for early damage identification and assessment. Statistical indices, such as Root Mean Square Deviation (RMSD) and moving Root Mean Square Deviation (mRMSD), were used to assess damage for each PZT transducer individually quantitatively. The results showed that the EMI signals generated by the SHM system during repeated four-point loading were sensitive to the initiation and propagation of crucial damage in the FRC prisms. The findings of this study show that the proposed approach could effectively detect and localize this damage.

2. Experimental Program

2.1. Materials

The ready-mix grade C30/37 concrete utilized in this study consists of a Type II-42.5 N Portland cement that conforms to the EN197-1 standard, coarse aggregate composed of crushed stone aggregates up to 16 mm, fine aggregate consisting of crushed limestone sand with a high fineness modulus, and water in a mass proportion of 1:2:2.4:0.52, respectively. The main mechanical properties of the used concrete were obtained by supplementary testing performed in this study: Density of the concrete mix 2355 Kg/m^3, modulus of elasticity 43 GPa, mean compressive strength 46 MPa, and mean modulus of rupture 4.2 MPa.

Macro synthetic fibers of polyolefin, whose length was 50 mm and equivalent diameter was 0.715 µm, were mixed into the fresh concrete batch. According to the manufacturer's specifications, Young's modulus under tension and the tensile strength of the fibers were 6 GPa and 430 MPa, respectively. The synthetic fibers were added at a rate of 5 kg per 1 m^3 of concrete during the mixing procedure and are commercially known as SikaFiber Force 50 (Figure 1).

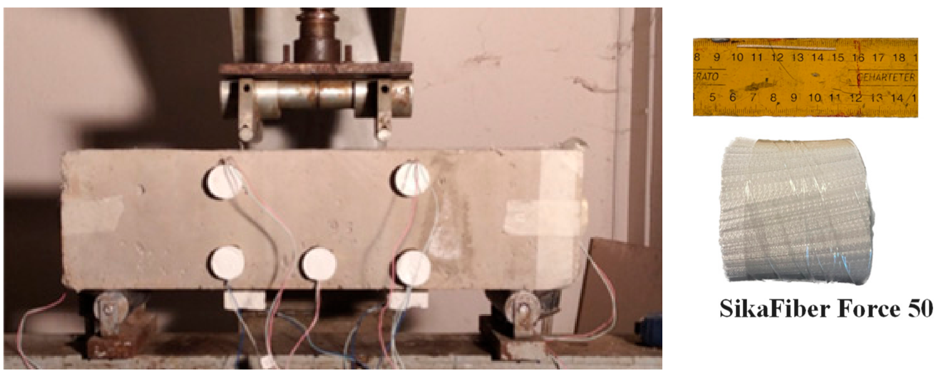

(a) (b)

Figure 1. Materials: (**a**) FRC specimens; (**b**) macro synthetic fibers.

The fibers were carefully placed into the pan to ensure uniform fiber distribution and maintain the fluidity of the fresh FRC mixture. Moreover, the macro synthetic fibers were gradually added by hand in small increments while stirring to prevent the formation of clumps. During the stirring of the mixture, the components were gradually homogenized, the blend became maneuverable, and the fibers dispersed, preventing segregation in the FRC and ensuring a homogeneous internal distribution in all directions. Then, the FRC mixture was molded and appropriately vibrated.

2.2. Tests and Specimens

Three FRC prismatic specimens measuring 450 mm in length, 150 mm in height, and 150 mm in width were evaluated in the standard four-point bending configuration, as depicted in Figure 2. The FRC specimens were supported at both ends over a span length of 450mm, and the two linear loads were enforced at a 75 mm distance on each side of the specimen's top surface using two hardened steel rollers. The three specimens were subjected to a four-point bending test, following the guidelines of ASTM C78 [26], to determine the fracture behavior of the concrete using a servo-controlled hydraulic machine.

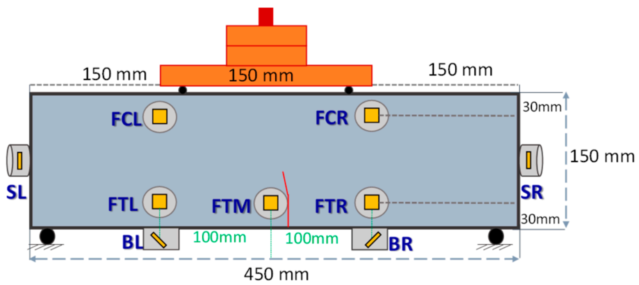

(**a**)

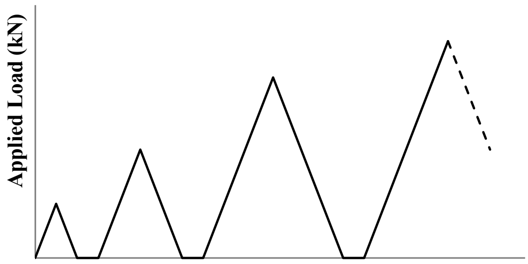

(**b**)

Figure 2. (**a**) Test setup and PZTs configuration, and (**b**) loading sequence of the tested specimens.

Figure 2 illustrates the loading sequence of the tested FRC specimens in terms of applied load versus loading cycle. Specifically, the FRC specimens were subjected to repeated four-point load (loading, unloading, reloading, etc.) at three different load/stress levels prior to total failure that equal to (a) 1 MPa, (b) 2 MPa, and (c) 3.3 MPa, corresponding to the 25%, 50%, and 83% of the final failure that is approximately equal to 4 MPa. Each selected loading step reflects an estimated specimen condition, respectively: (a) almost intact, elastic response, (b) minor, non-visible internal damage, and (c) significant internal cracking and deterioration. Specimens were finally reloaded until failure due to the formation of their fatal crack in the midspan of the specimens, as depicted in Figure 3. The ratio of maximum flexural strength is outlined in Table 1.

Table 1. Examined load levels and ratio of the max flexural strength.

	Load Step	Specimen 1	Specimen 2	Specimen 3
Flexural stress (MPa)	1	1.0	1.0	1.0
	2	2.0	2.0	2.0
	3	3.3	3.3	3.3
	4	4.8	4.0	3.9
Ultimate damage level	1	UL_1MPa	UL_1MPa	UL_1MPa
	2	UL_2MPa	UL_2MPa	UL_2MPa
	3	UL_3.3MPa	UL_3.3MPa	UL_3.3MPa
	4	Failure_4.8MPa	Failure_4MPa	Failure_3.9MPa
The ratio of the max flexural strength	1	21%	25%	25%
	2	42%	50%	51%
	3	69%	83%	85%
	4	Failure	Failure	Failure

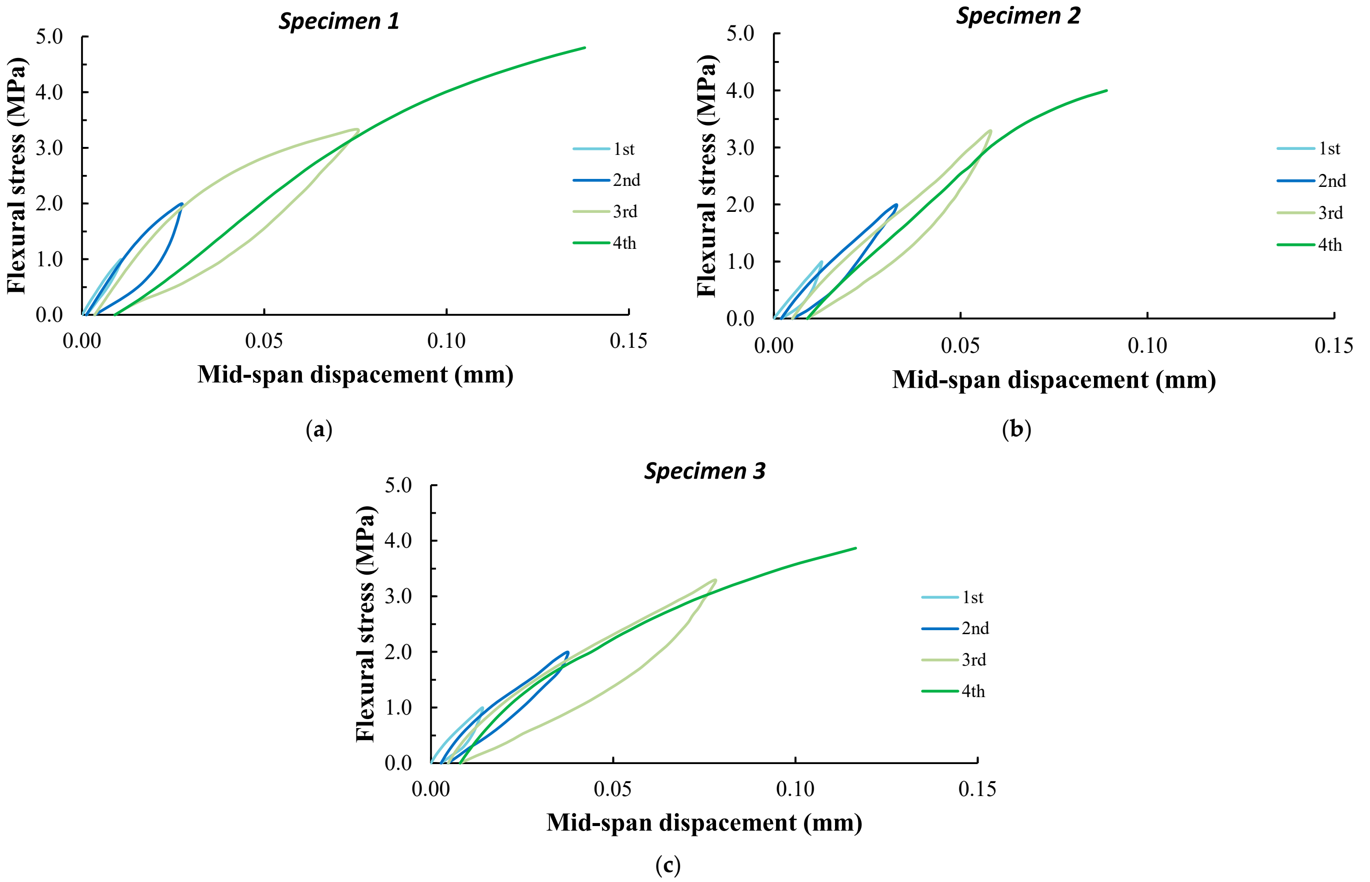

Figure 3. Experimental behavior; (**a**) Specimen 1, (**b**) Specimen 2, and (**c**) Specimen 3.

The four-point tests were conducted using force control to achieve the desired load for each ultimate damage level (Table 1). Load and mid-span deflection data were continuously acquired during the tests throughout the Load cell and the Model LE Laser Extensometers. The experimental performance in terms of flexural stress versus mid-span deflection performance and cracking pattern of Specimen 1, Specimen 2, and Specimen 3 are illustrated in Figure 3.

2.3. SHM Technique and PZT Transducer Configuration

This experimental study employed a wireless SHM and damage-detection system based on the EMI method. Real-time measurements of the EMI were performed using a custom-made device called a "Wireless impedance/Admittance Monitoring System (WiAMS)" and a network of PZT transducers. These devices have been extensively presented in various experimental programs by [20–22,26,27], proving their efficacy in detecting and evaluating damage severity in RC and FRC structural members. The theoretical components and additional information about the proposed SHM system can be found in [28,29].

Specifically, this study examined the application of the EMI method to identify damage in FRC structural members caused by cracking during repeated loading in four-point bending tests. In addition, the widely acknowledged advantages of PZT transducers, particularly their ability to function as transducers that undergo vibration when exposed to amplified harmonic excitation voltage while also serving as sensors that detect reflected waves through electrical impedance frequency response, were employed.

PZT transducers used in tested specimens, with dimensions of 20 mm × 20 mm × 5 mm, were first coated with cement paste and then externally epoxy bonded at the surface of the tested specimens. The influence of the angle created between the direction of the formed crack and the direction of the PZT's polarization is also investigated. For this purpose, two PZTs for each specimen were coated with the cement paste at a predefined angle of around 45°. Furthermore, the position of the PZT transducers on the surface of the specimens, which is related to the distance from the critical crack and its influence on the SHM technique's efficiency, is also examined.

After casting and demolding the FRC specimens, cement paste-coated PZT transducers were carefully epoxy bonded on the surface of the specimens at different positions. These specially coated piezoelectric patches have been manufactured to operate efficiently with the wireless EMI-based SHM system and to be reused after the failure of the examined specimen. The positioning selection has been applied relative to the expected location of the potential cracking and fatal failure. Nine PZT patches were epoxy bonded to the surface of each tested specimen, as shown in Figure 4. The characteristics and positions of the installed PZT transducers in all tested specimens are the same. The notation (code-names) of each PZT patch according to its position is as follows (see also Figures 2 and 4):

- One PZT patch was bonded in the middle of the facade of the specimen, in the tension zone (FTM: Facade Tension Middle);
- Two PZT patches were bonded on the right side of the facade of the prism at a 100 mm distance from the middle of the specimen; one in the tension zone (FTR: Facade Tension Right) and one in the compression zone (FCR: Facade Compression Right);
- Two PZT patches were bonded on the left side of the facade of the prism at a 100 mm distance from the middle of the specimen; one in the tension zone (FTL: Facade Tension Left) and one in the compression zone (FCL: Facade Compression Left);
- Two PZT patches were bonded to the bottom of the prism, one on the right side (BR: Bottom Right) and one on the left side (BL: Bottom Left), each at a 100 mm distance from the middle of the specimen. Both transducers (BL and BR) were cast at a 45° predefined angle;
- Two PZT patches were bonded to the mid-height and mid-width of each side of the prism; one on the right side (SR: Side Right) and one on the left side (SL: Side Left).

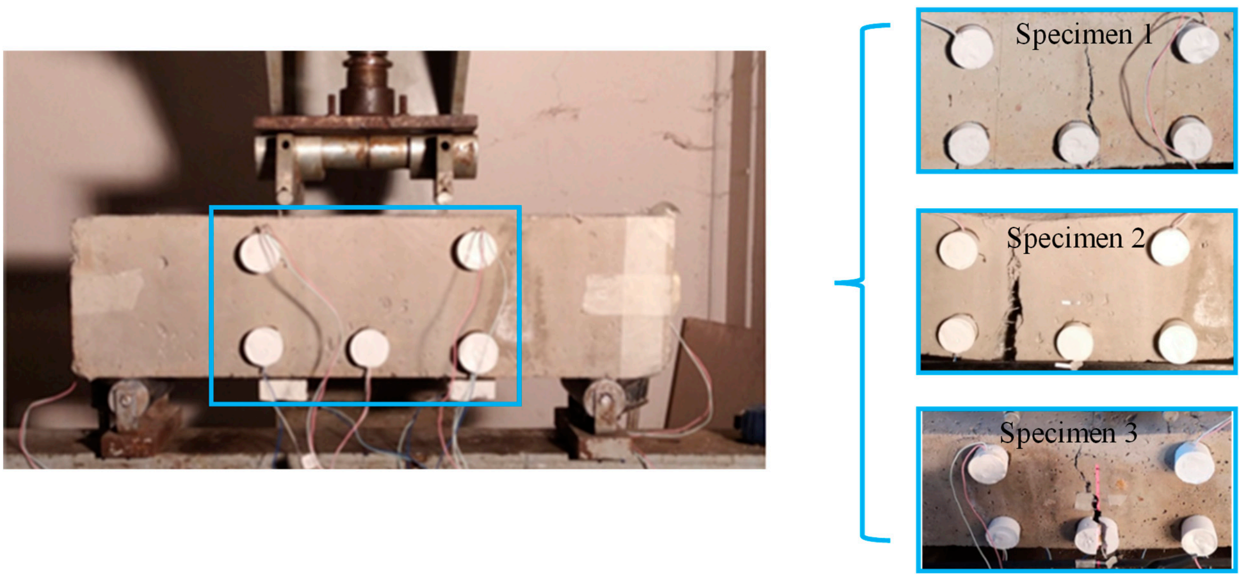

(**a**) (**b**)

Figure 4. (**a**) Test rig, instrumentation, and configuration of the PZT transducers mounted to the FRC specimens and (**b**) cracking pattern at the failure of the three tested FRC specimens.

3. Results and Discussion

3.1. Damage Quantification

EMI measurements were performed using WiAMS devices at 2.5 V excitation voltage in a board-wide frequency spectrum ranging from 10 to 250 kHz. During loading, typical voltage curves for all PZT transducers were extracted from these devices at each loading damage level (after unloading) to expunge induced stress variations.

It is known that the comparison of the differences between the healthy typical voltage curve and every relevant one in the following damage level could not be competent enough to determine damage detection. Therefore, the application of a sufficient quantitative assessment of damage is essential. For this purpose, the traditionally used damage index of RMSD is applied. The expression of the traditional RMSD index is presented below in the above equation:

$$\mathrm{RMSD} = \sqrt{\frac{\sum_1^M \left(\left|V_p(f_r)\right|_D - \left|V_p(f_r)\right|_0\right)^2}{\sum_1^M \left(\left|V_p(f_r)\right|_0\right)^2}} \tag{1}$$

where $\left|V_p(f_r)\right|_0$ is the absolute value of the voltage output signal as extracted from the PZT transducer at the healthy pristine state of the specimen in a specific frequency f_r, $\left|V_p(f_r)\right|_D$ is the absolute value of the corresponding voltage output signal as measured from the same PZT at any damage level, and M is the number of measurements in the frequency band of 10–260 kHz.

Moreover, a relatively new dynamic metric index proposed recently in the literature [30] is also addressed as an additional supplemental tool to achieve higher efficiency and accuracy in damage detection of the FRC specimens of this study. The expression of this new index, namely as “moving RMSD” (mRMSD), is given as:

$$\mathrm{mRMSD}_{\mathrm{a=1,b-n}} = \sqrt{\frac{\sum_{\alpha=1}^n \left(\left|V_p(f_r)\right|_D - \left|V_p(f_r)\right|_0\right)^2}{\sum_{\alpha=1}^n \left(\left|V_p(f_r)\right|_0\right)^2}} \tag{2}$$

where b and n are the number of data points in the compared signature and moving frame, respectively. A preliminary setup of the frequency range at 50 kHz has been selected before applying the mRMSD index to the moving frame.

3.2. Voltage and Indices Analysis

The tested specimens exhibited predictable flexural response and brittle failure, as they were designed according to the test method. Typically, the fatal flexural crack formed in the mid-span and perpendicular to the specimen’s longitudinal axis (see each specimen’s cracking pattern at failure in Figure 3). For comparison reasons, the PZT transducers were categorized into four groups according to their polarization direction towards the critical crack at the failure. These four groups of the PZTs are comprised of (a) BL and BR; (b) SL and SR; (c) FTL, FTR, and FTM; and (d) FCL and FCR transducers.

An effort to recognize the similarities and differences between the responses of the grouped PZT transducers is also attempted using the values of the adopted indices. Typical curves of the PZT voltage frequency responses and the ratio of the RMSD and mRMSD indices of each PZT transducer are presented for each specimen.

3.2.1. Specimen 1

In Specimen 1, the fatal failure was formed slightly right in the mid-span. PZTs BL and BR were positioned at a predefined angle of 45° in a vertical polarization direction to the expected and finally developed fatal failure, as shown in Figure 4. Figure 5 shows the voltage frequency discrepancies between the healthy curve and every relevant one in the following damage level for the PZTs BL and BR. These discrepancies are noticeably more significant for the BR PZT showing the damage on the specimen’s right side. Also, PZT BR showed a gradual and considerable ascending of values in the index of RMSD in comparison to its symmetric BL transducer, as shown in Figure 6, at every damage level. Figure 6 illustrates the mRMSD plots of the PZTS BL and BR, where PZT’s BR signature showed an upward trend compared to its symmetric BL transducer at every damage level.

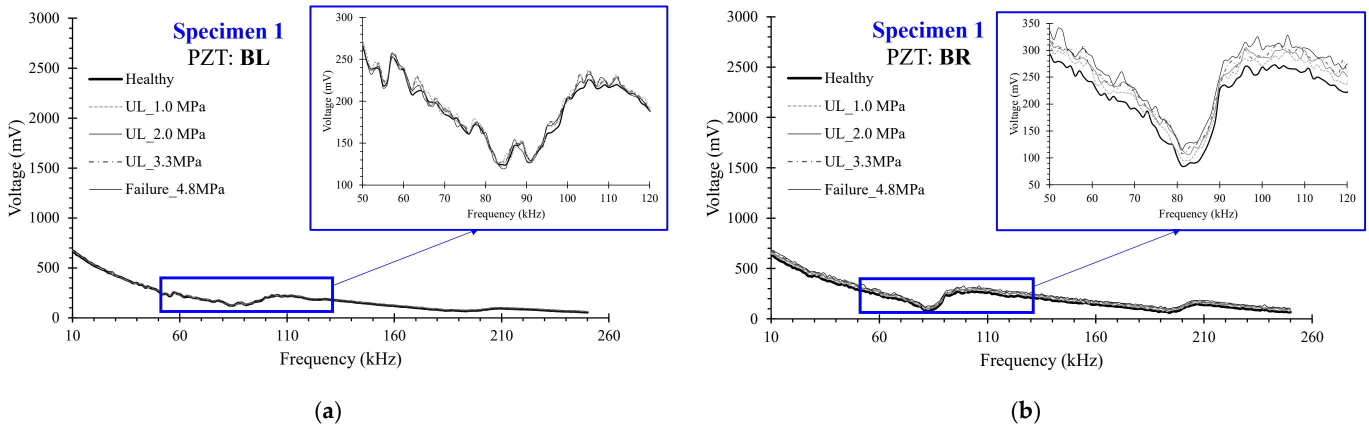

Figure 5. Typical voltage frequency response of the PZT (**a**) BL and (**b**) BR bonded to Specimen 1 under repeated flexural loading.

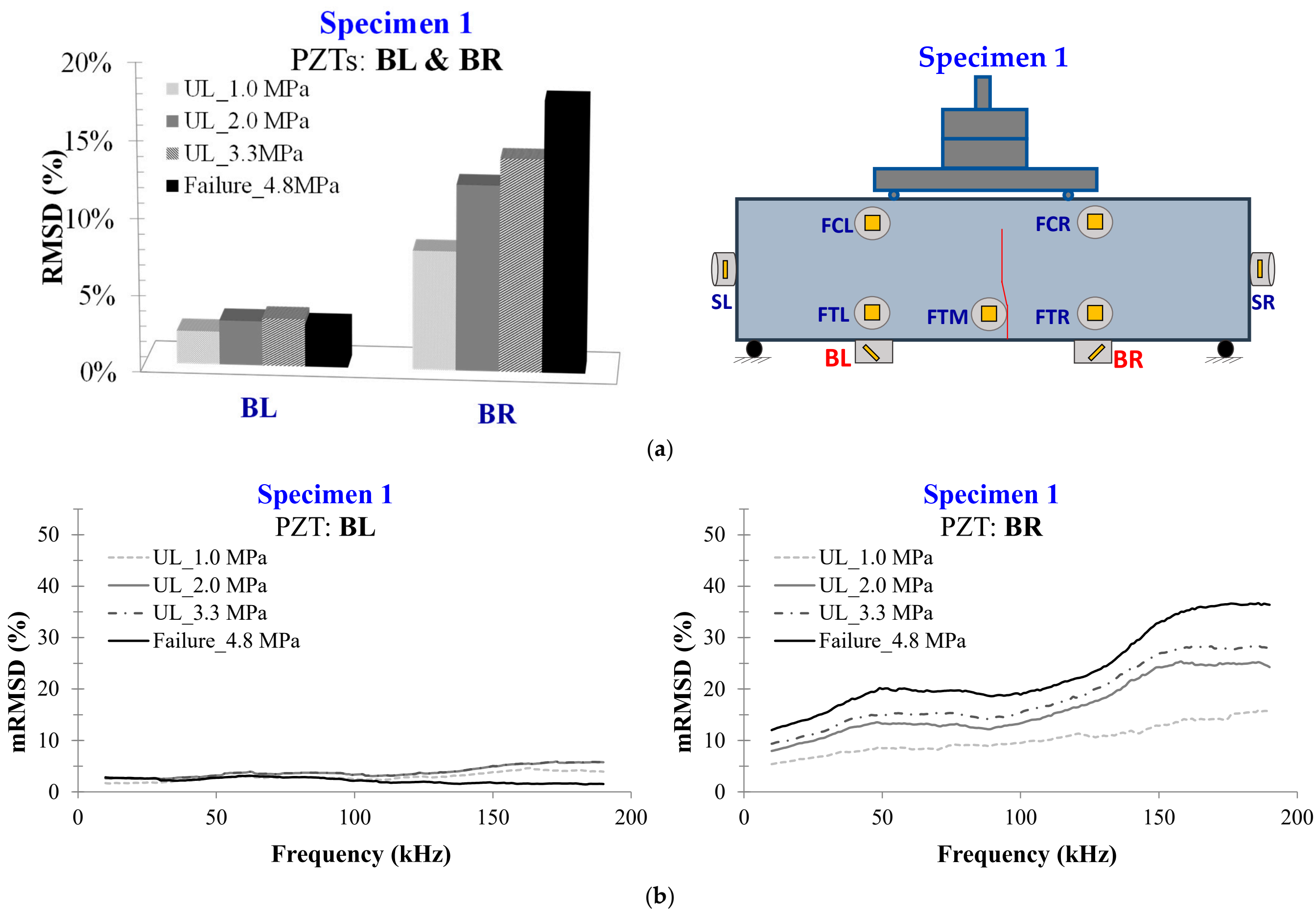

Figure 6. Damage assessment measurements in terms of (**a**) RMSD index ratio and (**b**) mRMSD index ratio of the PZT BL and BR bonded to Specimen 1.

PZTs FCR and FCL were bonded in a symmetric position having parallel polarization direction to the finally formed failure, as shown in Figure 4. Figure 7 presented the voltage frequency response of the PZT FCR and FCL, where more significant discrepancies were observed for the PZT FCR, which is located on the side closer to the crack. The relevant response has the RMSD and mRMSD values depicted in Figure 8. PZT FCR showed increased RMSD values at the second to last damage level UL_3.3MPa than FCL, as shown in Figure 8. Moreover, the PZT FCR voltage frequency response and the ratio of the RMSD and mRMSD indices showed an upward trend compared to its symmetric FCL transducer at every damage level.

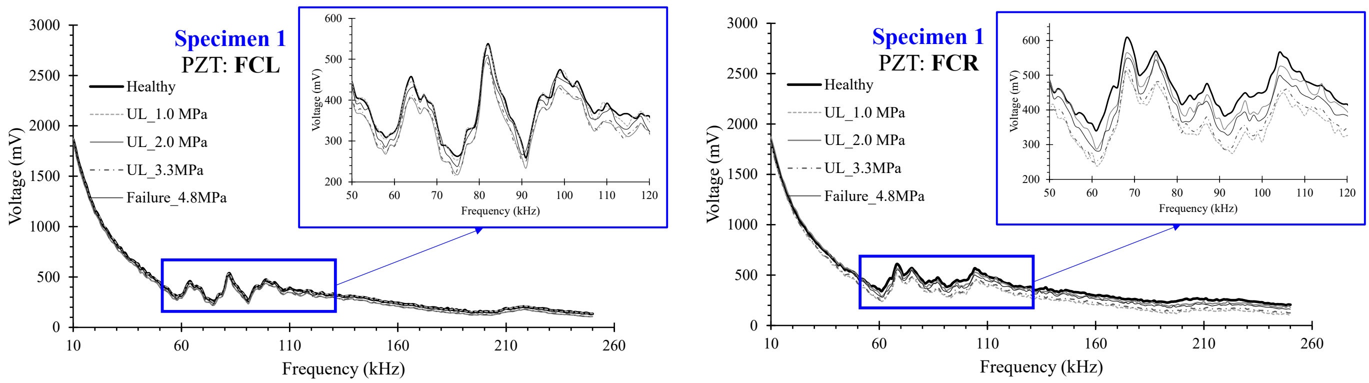

(**a**) (**b**)

Figure 7. Typical voltage frequency response of the PZT (**a**) FCL and (**b**) FCR bonded to Specimen 1 under repeated flexural loading.

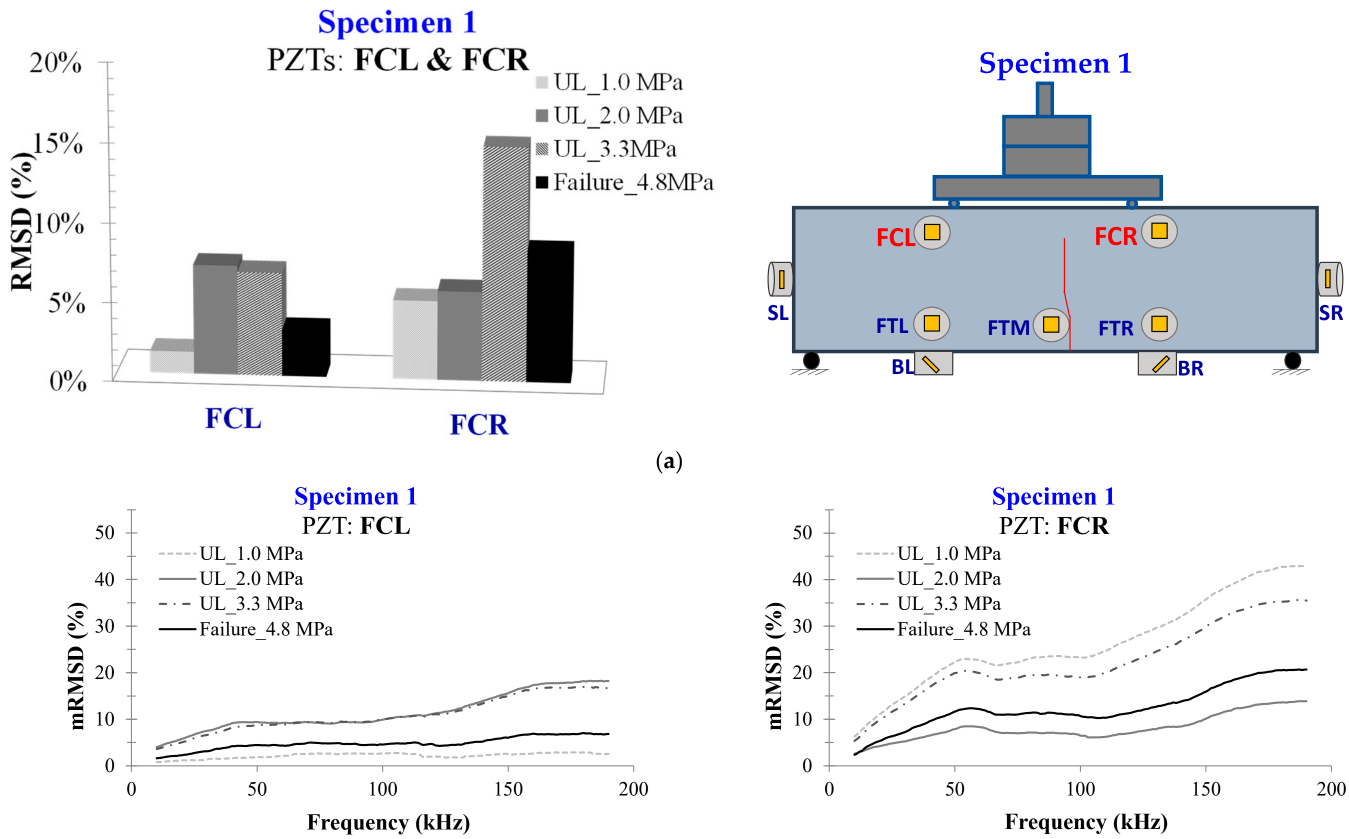

(**a**)

(**b**)

Figure 8. Damage assessment measurements in terms of (**a**) RMSD index ratio and (**b**) mRMSD index ratio of the PZT FCL and FCR bonded to Specimen 1.

PZTs FTR, FTM, and FTL were placed in the mid-span tensional zone to the right, middle, and left. All these PZTs had parallel polarization direction to the finally formed failure. FTM and FTL showed differences between the voltage responses due to the damage on the right side in Figure 9. FTM showed a steep ascending of the RMSD index at damage state UL_3.3MPa. At the same time, FTR and FTL followed a gradual rise of the RMSD and mRMSD indices, as shown in Figure 10.

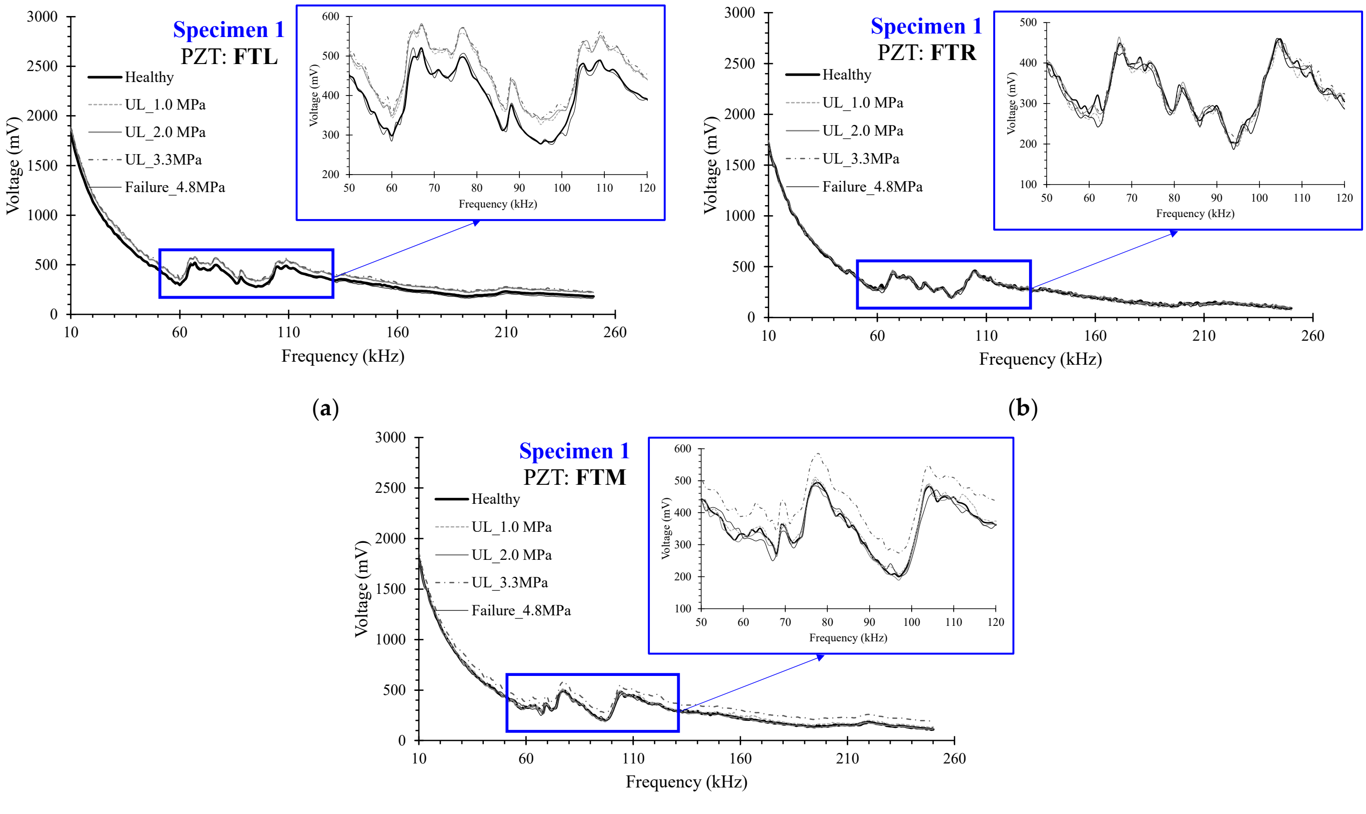

Figure 9. Typical voltage frequency response of the PZT (**a**) FTL, (**b**) FTR, and (**c**) FTM bonded to Specimen 1 under repeated flexural loading.

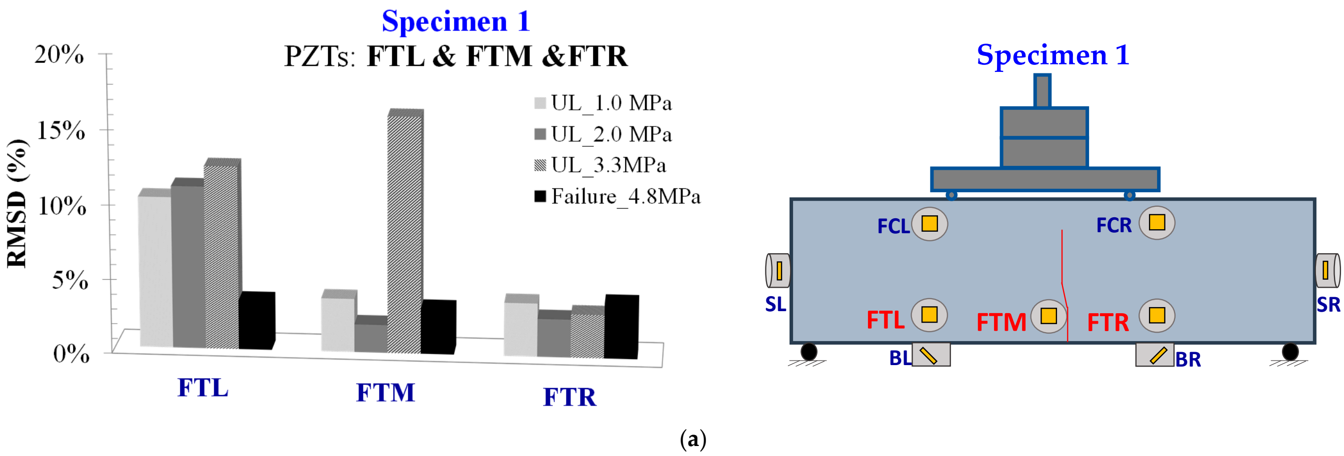

Figure 10. *Cont.*

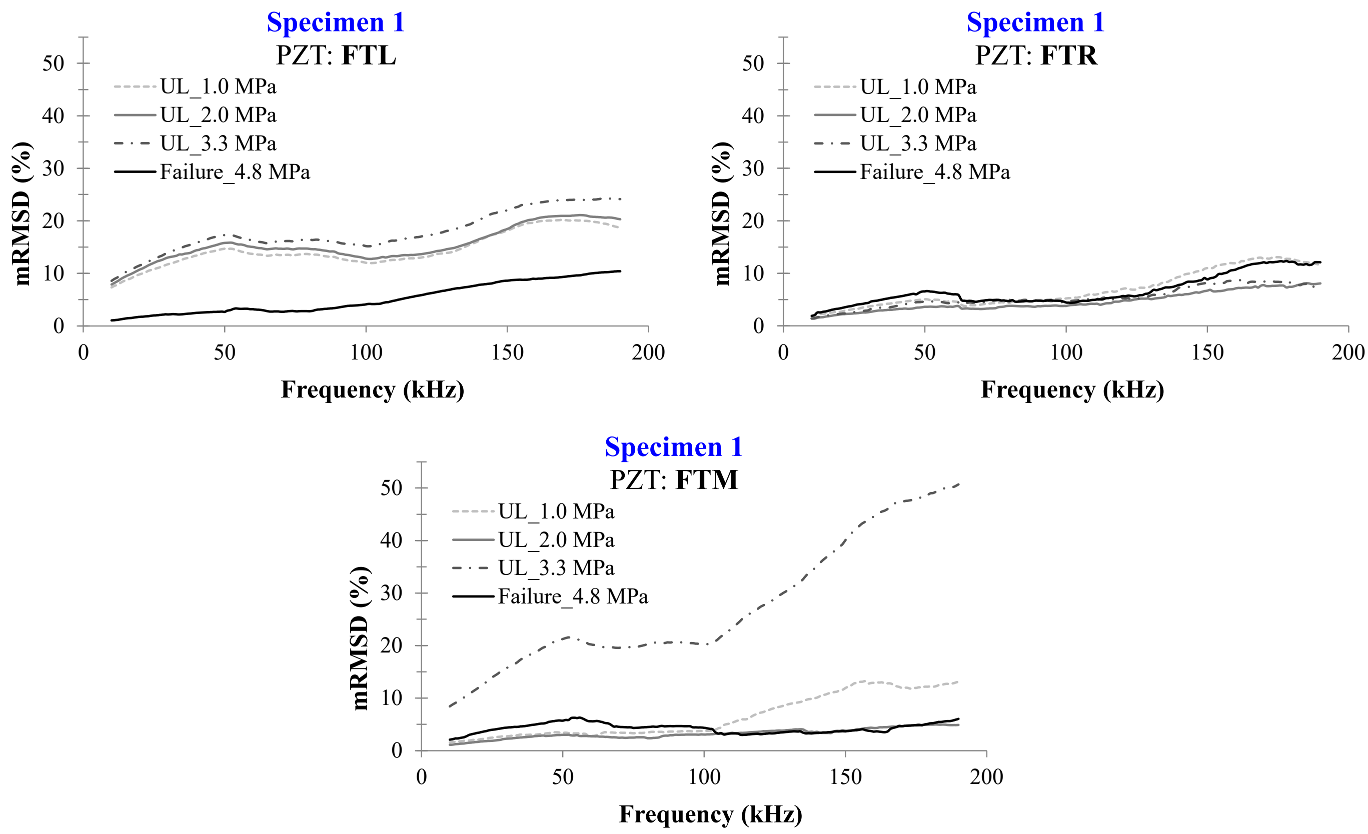

(**b**)

Figure 10. Damage assessment measurements in terms of (**a**) RMSD index ratio and (**b**) mRMSD index ratio of the PZT FTL, FTR, and FTM bonded to Specimen 1.

PZTs SR and SL were bonded to the external sides of the specimens and positioned in a vertical polarization direction to the failure, and they indicated almost equal RMSD values. These PZTs were bonded to ensure monitoring of the area in case of an unexpected failure pattern. However, some interesting results can be extracted as both transducers converge to a similar final value of the RMSD index for all levels of damage. PZT SR and SL show almost similar voltage frequency responses in Figure 11 despite the SR delivering a steep ascending of the RMSD index. Figure 12 illustrates the mRMSD plots where it can be observed that the trends are almost the same.

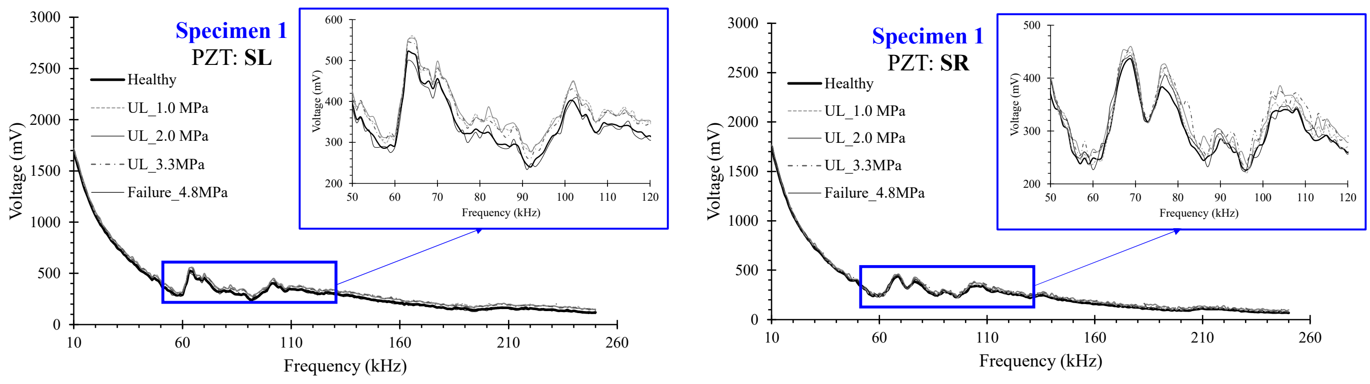

(**a**) (**b**)

Figure 11. Typical voltage frequency response of the PZT (**a**) SL and (**b**) SR bonded to Specimen 1 under repeated flexural loading.

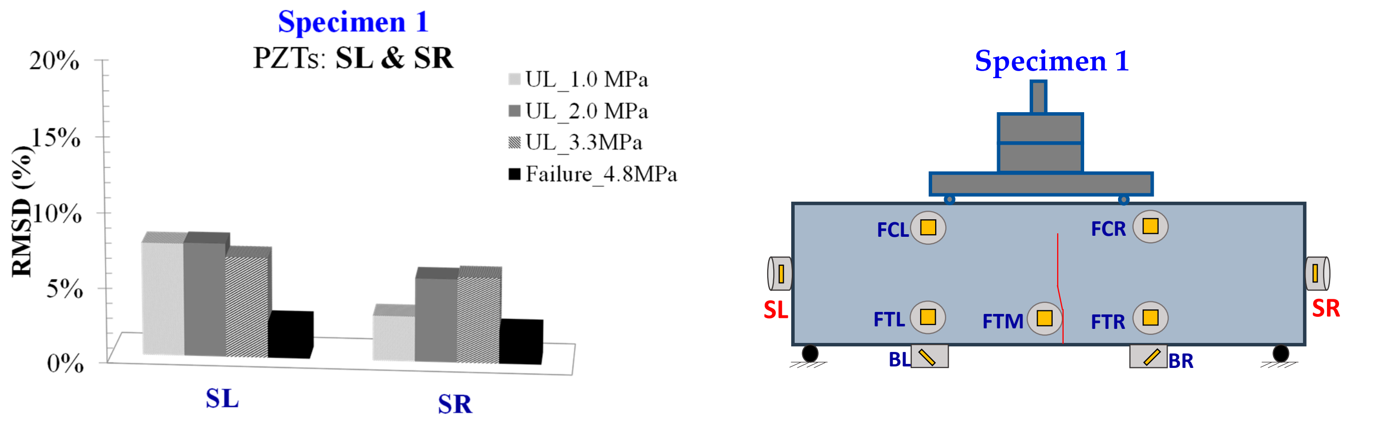

(a)

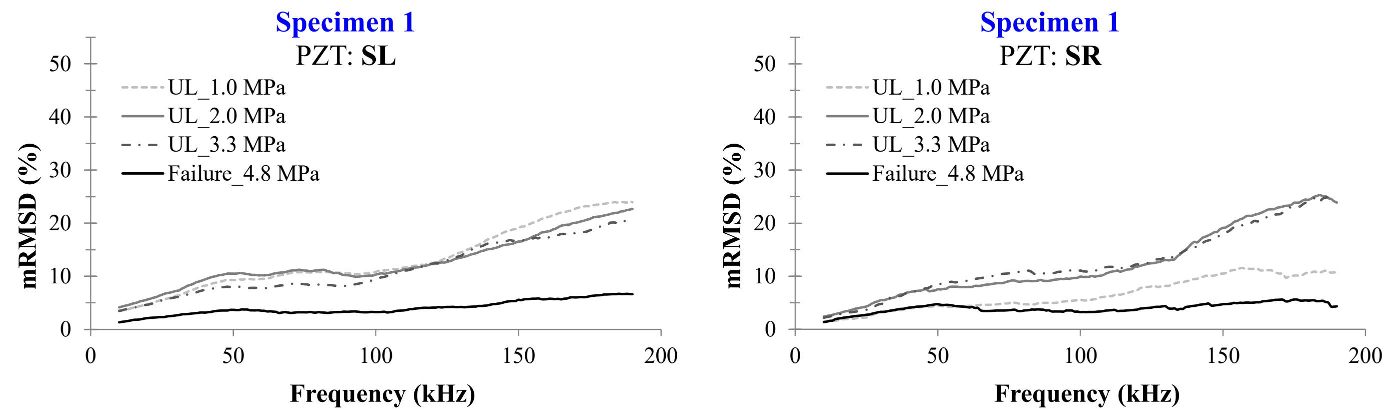

(b)

Figure 12. Damage assessment measurements in terms of (**a**) RMSD index ratio and (**b**) mRMSD index ratio of the PZT FCL and FCR bonded to Specimen 1.

3.2.2. Specimen 2

In Specimen 2, the fatal failure was formed 40 mm left from the mid-span. PZTs BL and BR were positioned at a predefined angle of 45° in a vertical polarization direction to the expected failure. Figure 13 illustrates the voltage frequency discrepancies between the healthy curve and every relevant one in the next damage level for the BL and BR PZT, respectively. The distinctions are noticeably more significant for the BL PZT. Also, PZT BL showed significantly ascending values of indices RMSD and mRMSD even in early damage levels compared to its symmetric BR transducer. However, BR also seemed to be sensitive to the formed crack, as shown in Figure 14.

Moreover, Figures 13 and 14 demonstrate a progressively increasing response on the left side for the initial three damage levels. Finally, an increasing trend is observed on the specimen's left side, both from the PZTS voltage frequency responses and the statistical indices ratio, mainly in the first three levels. In the failure damage level, an abrupt decline in the indices ratios was observed, perhaps due to the limitation of the sensor range due to the final crack.

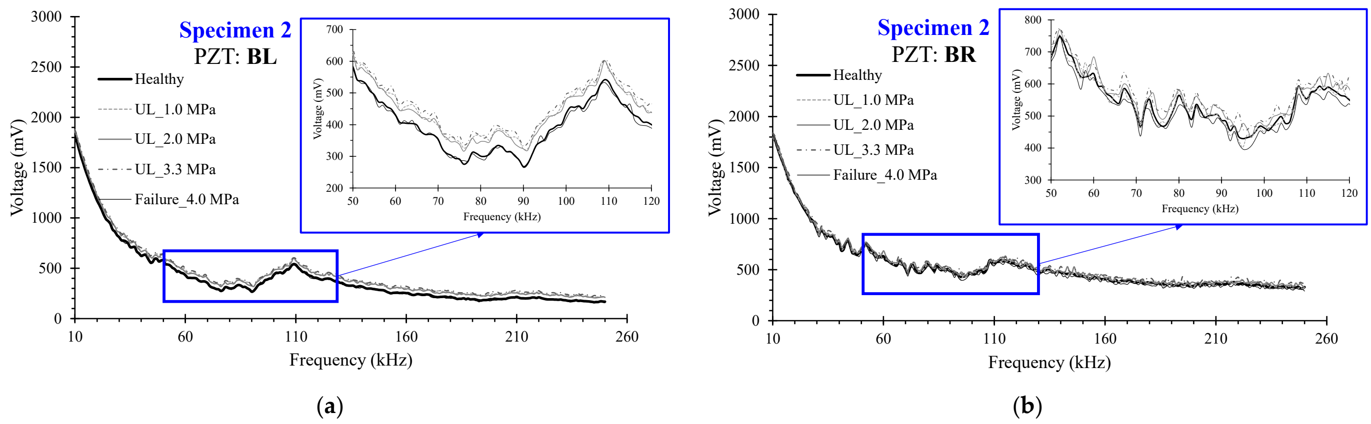

Figure 13. Typical voltage frequency response of the PZT (**a**) BL and (**b**) BR bonded to Specimen 2 under repeated flexural loading.

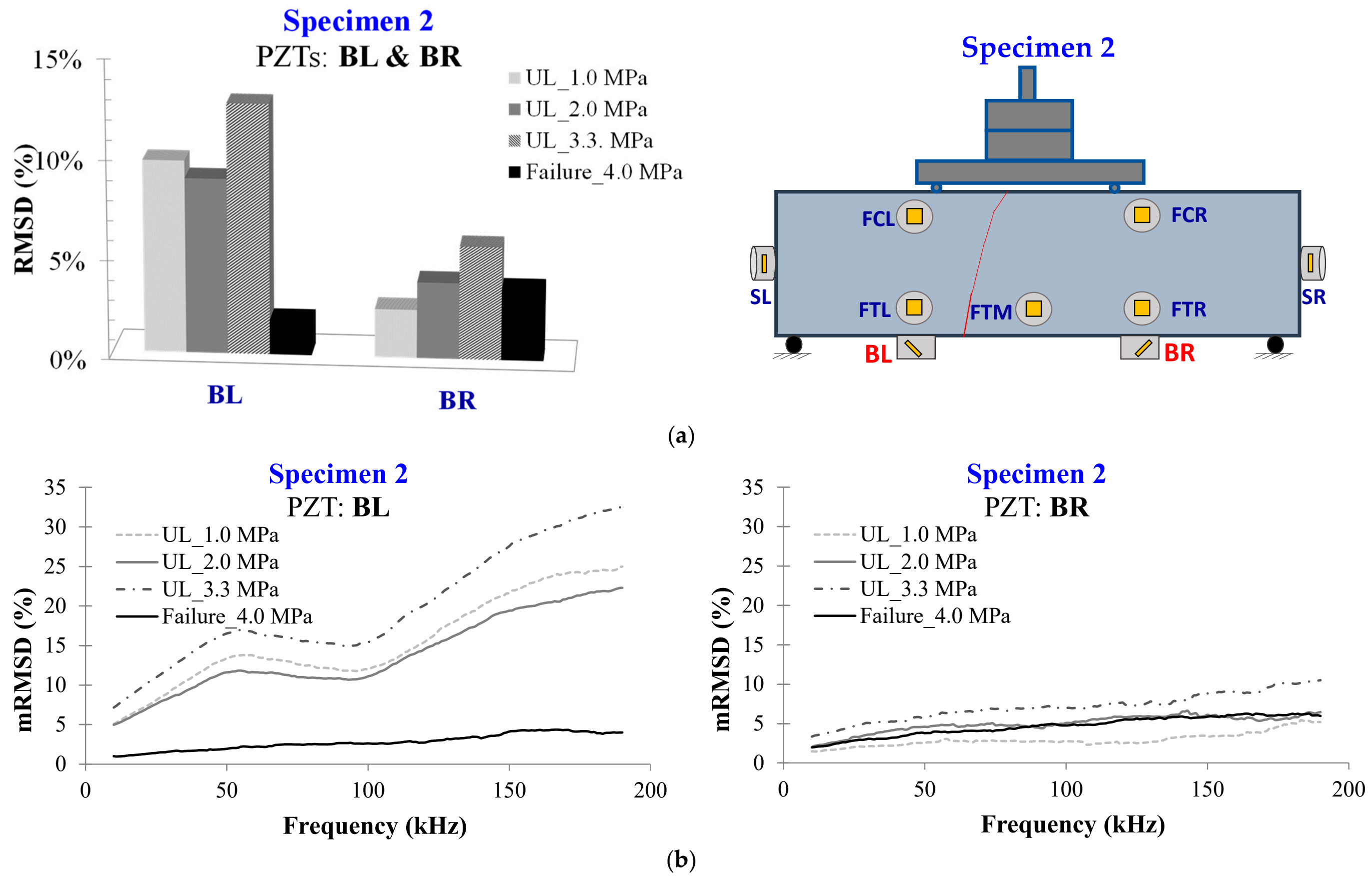

Figure 14. Damage assessment measurements in terms of (**a**) RMSD index ratio and (**b**) mRMSD index ratio of the PZT BL and BR bonded to Specimen 2.

PZTs FCR and FCL were bonded in a symmetric position having parallel polarization direction to the finally formed failure. Both of these PZTs showed to be influenced only at the last damage level. FCR and FCL show similar voltage responses, as shown in Figure 15, despite the FCR showing a slightly significant discrepancy at the final damage state. As a result, FCR exhibited slightly higher RMSD and mRMSD values at the last damage level, as shown in Figure 16, and this is probably caused due to the lateral to the right direction of the crack's propagation to the upper middle zone of the specimen. However, the RMSD values for the initial three damage levels are nearly the same, even though a slight difference at every damage state shows increased FCL RMSD ratios but slightly decreased FCR values of

RMSD. Figure 16 demonstrates that the mRMSD plots display a pattern of slight increases on the left side in all damage stages.

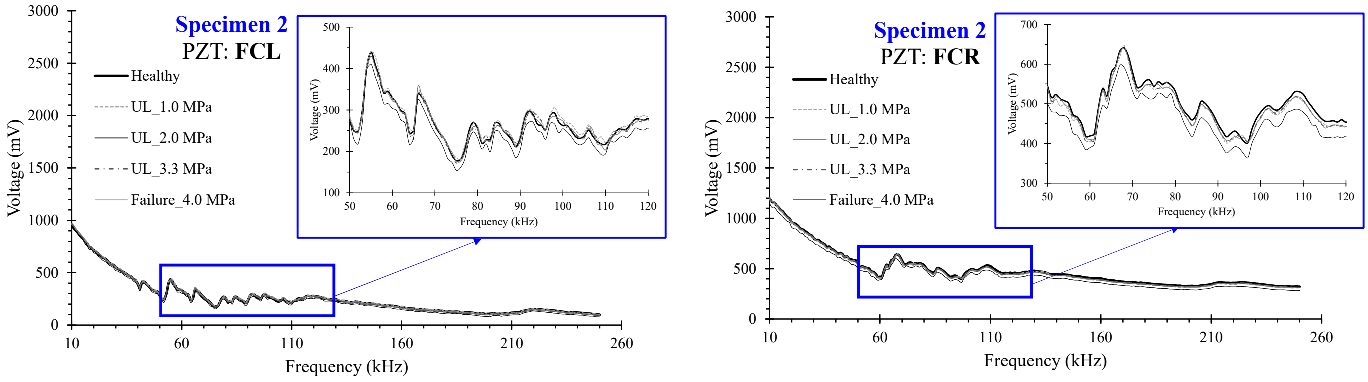

(**a**) (**b**)

Figure 15. Typical voltage frequency response of the PZT (**a**) FCL and (**b**) FCR bonded to Specimen 2 under repeated flexural loading.

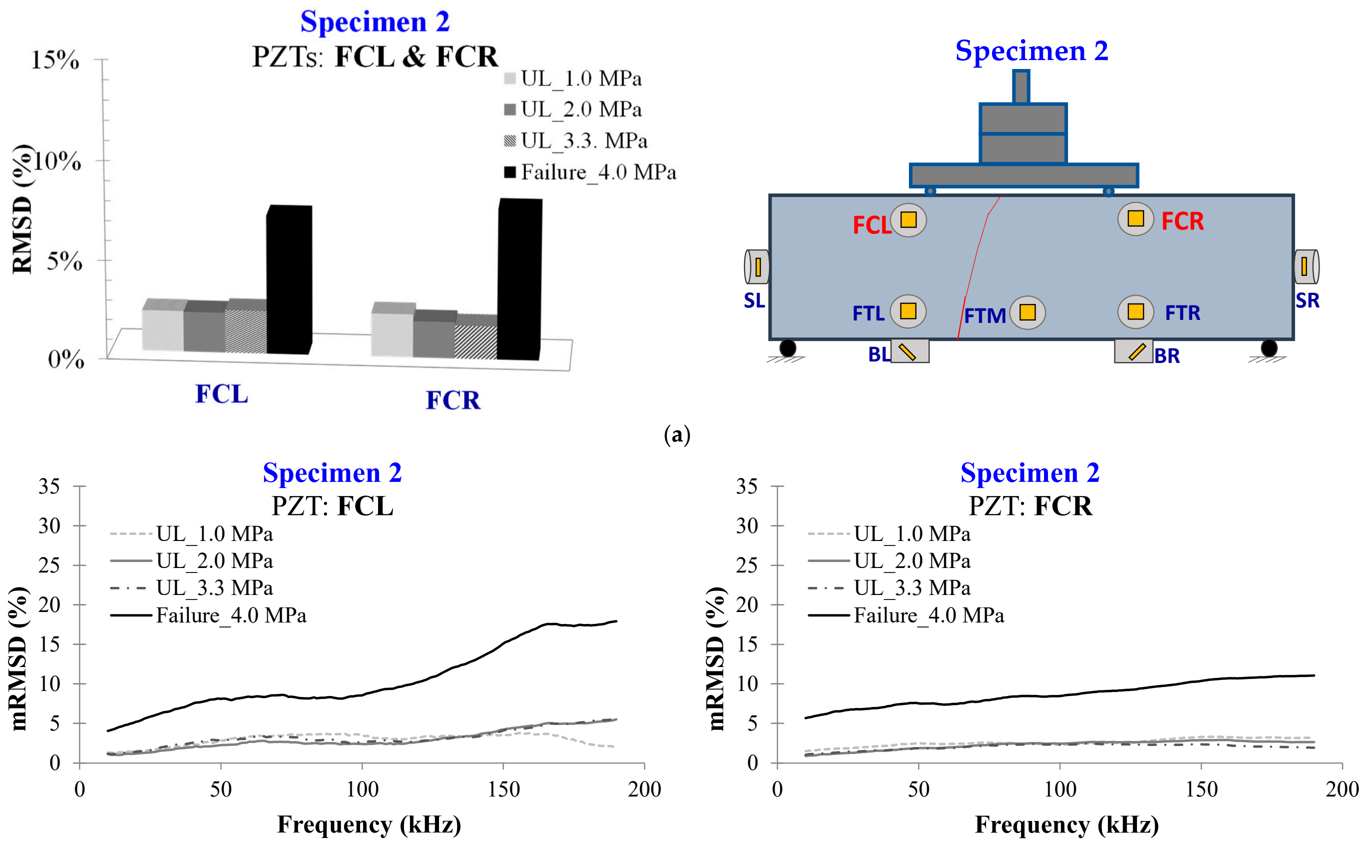

Figure 16. Damage assessment measurements in terms of (**a**) RMSD index ratio and (**b**) mRMSD index ratio of the PZT FCL and FCR bonded to Specimen 2.

PZTs FTR, FTM, and FTL were placed in the tensional zone to the right, middle, and left of the mid-span of Specimen 2, respectively. All the PZTs had parallel polarization direction to the finally formed failure. The recorded data of the transducers could not be employable enough as all the PZTs had similar voltage responses and RMSD and mRMSD values, as displayed in Figures 17 and 18, respectively. More significant discrepancies between the mRMSD signatures at FTM PZT can be observed in Figure 18.

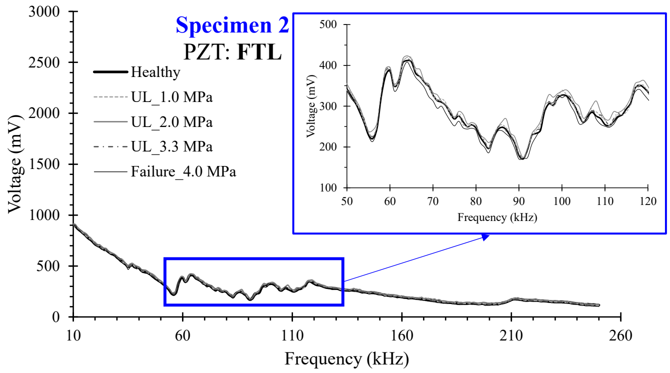

(**a**)

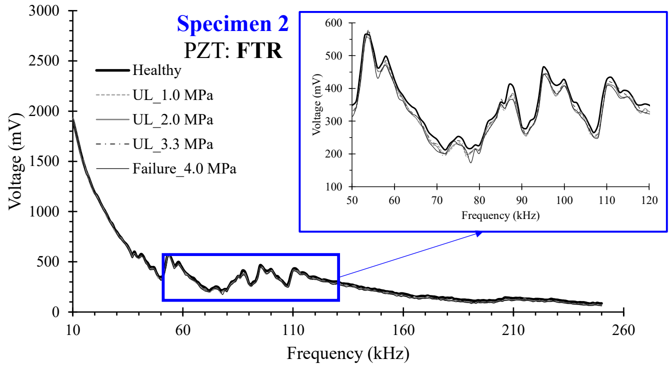

(**b**)

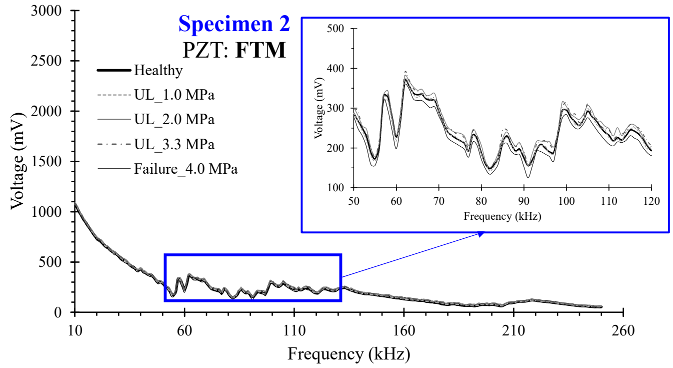

(**c**)

Figure 17. Typical voltage frequency response of the PZT (**a**) FTL, (**b**) FTR, and (**c**) FTM bonded to Specimen 2 under repeated flexural loading.

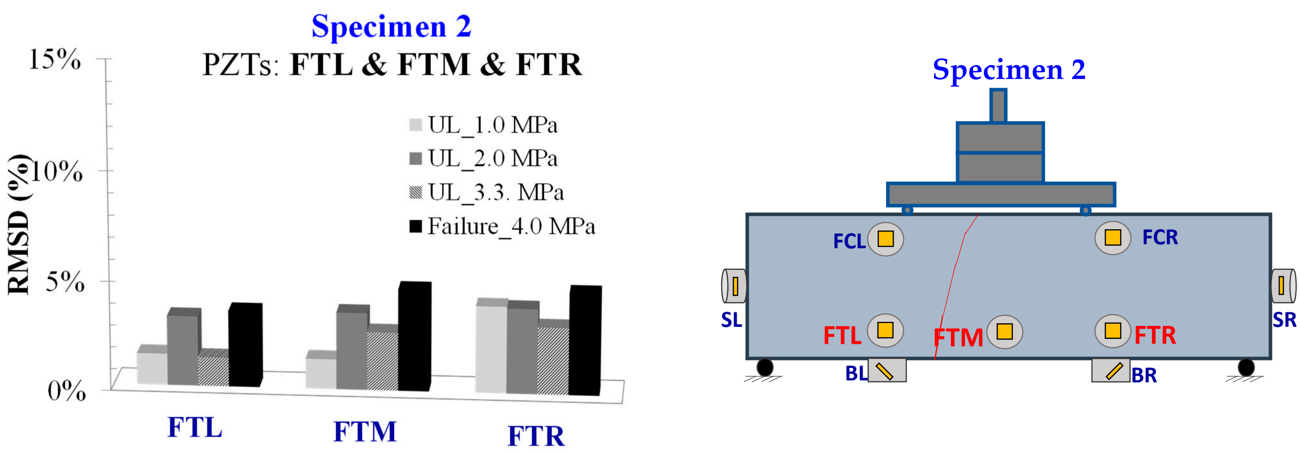

(**a**)

Figure 18. *Cont.*

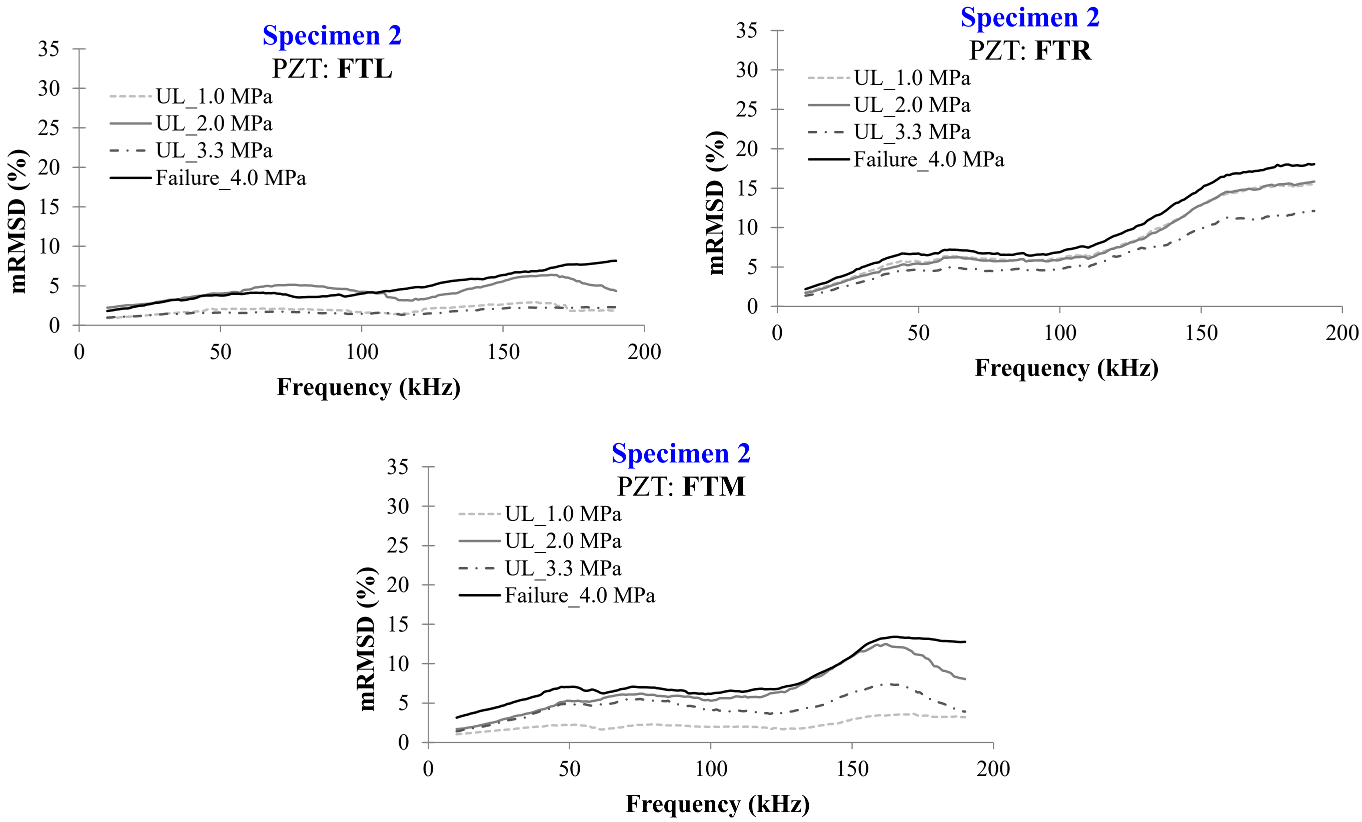

(**b**)

Figure 18. Damage assessment measurements in terms of (**a**) RMSD index ratio and (**b**) mRMSD index ratio of the PZT FTL, FTR, and FTM bonded to Specimen 2.

PZTs SR and SL were bonded to the outer sides and positioned in a vertical polarization direction to the expected failure. Both PZTs were bonded to ensure monitoring of the extreme areas in case of an unexpected out-of-the-mid-span fatal failure. Despite that, PZT SL seemed to have been influenced by the position of the fatal failure. Figure 19 shows a noticeable variation in voltage signatures across all damage stages, in contrast to the minor differences observed in SR PZT. Furthermore, the RMSD and mRMSD index values significantly increased at damage state UL_3.3MPa for the SL PZT, as shown in Figure 20. Conversely, PZT SR showed typical RMSD values considering that the failure was formed at a distance of limited monitoring capability.

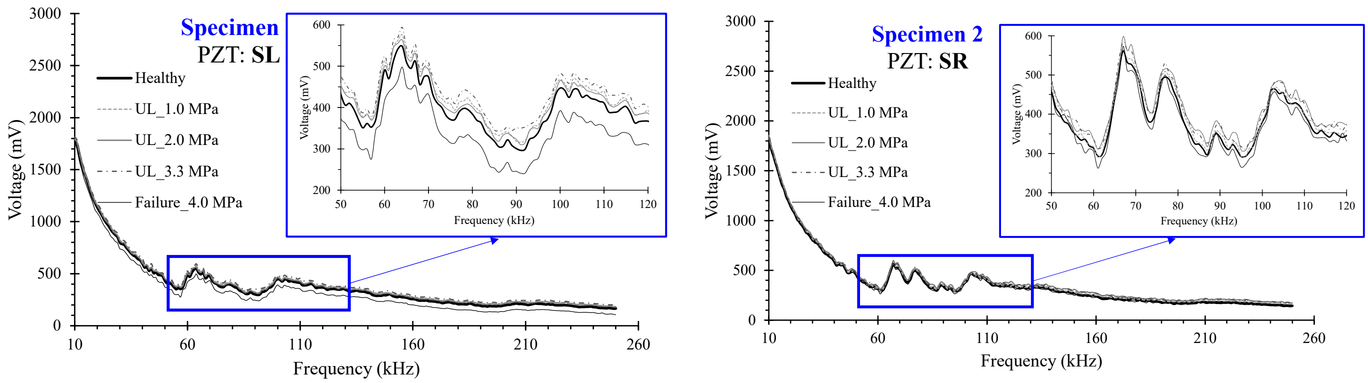

(**a**) (**b**)

Figure 19. Typical voltage frequency response of the PZT (**a**) SL and (**b**) SR bonded to Specimen 2 under repeated flexural loading.

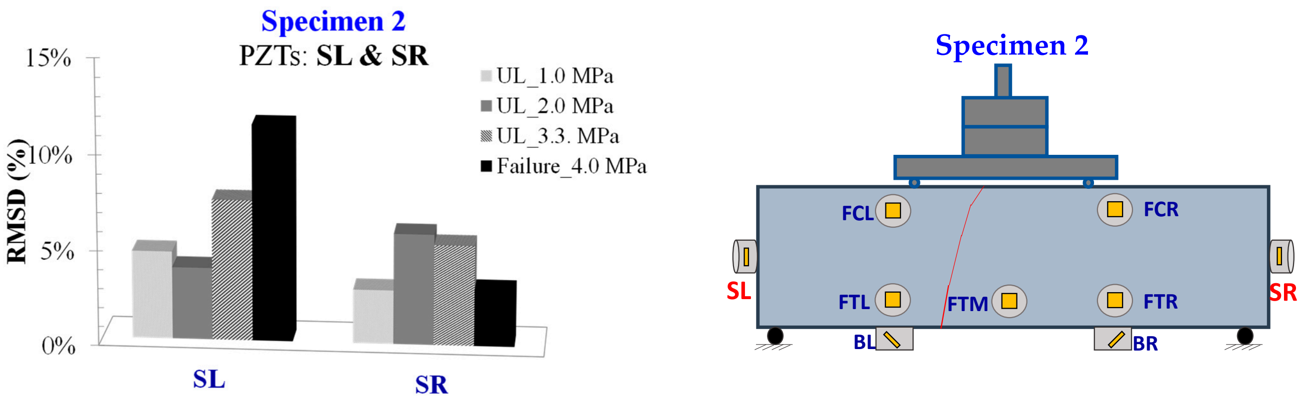

(**a**)

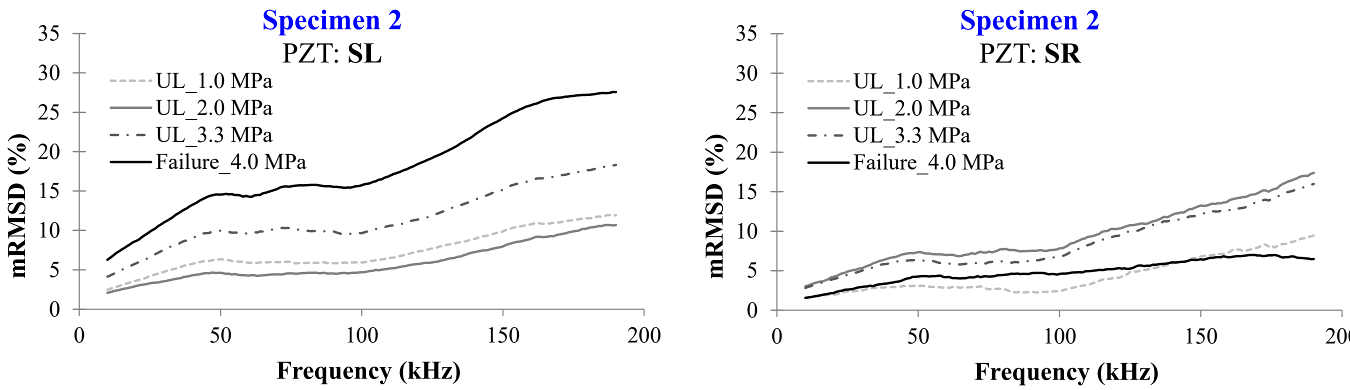

(**b**)

Figure 20. Damage assessment measurements in terms of (**a**) RMSD index ratio and (**b**) mRMSD index ratio of the PZT FCL and FCR bonded to Specimen 2.

PZTs are closer to fatal failure in comparison to the relevant symmetric of their group, alarms at earlier damage state, and have greater values of RMSD indices to the three out of four groups of PZTs. All the left PZTs in these groups seemed more sensitive and efficient than their symmetric left ones. It is crucial that the adjacent transducers responded satisfactorily to the failure, as there were no apparent cracks at this state.

3.2.3. Specimen 3

In Specimen 3, the fatal failure was caused in the mid-span, forming a lateral central direction from the bottom right to the upper left of the specimen. PZTs BL and BR were positioned at a predefined angle of 45° in a vertical polarization direction to the expected failure. Both PZTs showed significantly ascending values of indices. As depicted in Figure 21, PZT BL and BR show apparent discrepancies between the voltage response at the healthy state and all examined damage levels. Specifically, BR PZT, even at early damage levels UL_2MPa and UL_3.3MPa, demonstrated higher values of RMSD in comparison to its symmetric BL transducer (Figure 22). Since the failure occurred symmetrically in both transducers at the final damage level (Failure), equal values of the damage indices were observed. In Figure 22, the mRMSD values in the second and third levels of damage (UL_1MPa and UL_2MPa) showed a different form up to 100 kHz, but at the following damage levels, they showed almost similar behavior.

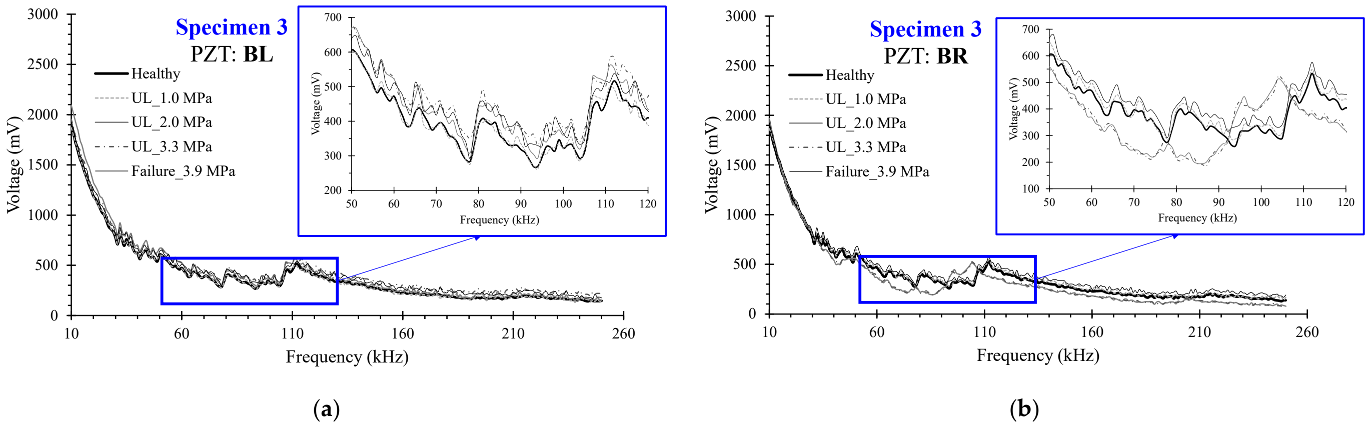

Figure 21. Typical voltage frequency response of the PZT (**a**) BL and (**b**) BR bonded to Specimen 3 under repeated flexural loading.

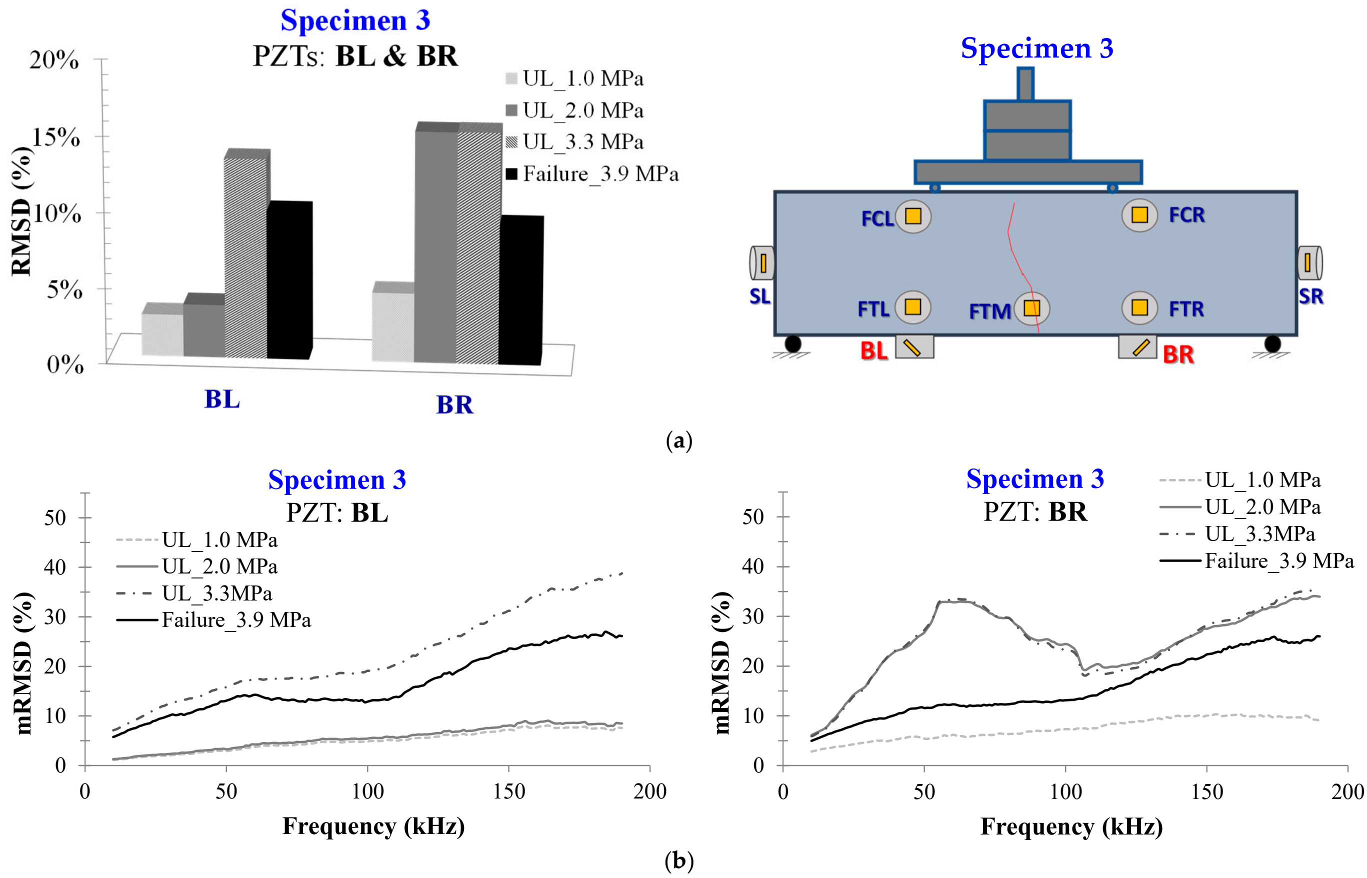

Figure 22. Damage assessment measurements in terms of (**a**) RMSD index ratio and (**b**) mRMSD index ratio of the PZT BL and BR bonded to Specimen 3.

The mRMSD values in the second and third levels of damage (UL_1MPa and UL_2MPa) exhibited a distinct pattern, as shown in Figure 22, particularly up to 100 kHz. However, at the following damage levels, their behavior became quite similar.

PZTs FCR and FCL were also bonded in a symmetric position having parallel polarization direction to the finally formed failure. The voltage signatures shown in Figure 23 display nearly similar discrepancies, with only minor variations at 150 kHz. As expected, both PZTs showed an equal RMSD index at the final damage level resulting from the transducers' symmetric position towards the formed failure. In Figure 24, the failure appears to have affected PZT FCR in earlier damage stages UL_2MPa and UL_3.3MPa. The same observation is also evident in Figure 24, where higher mRMSD values were observed in earlier damage states.

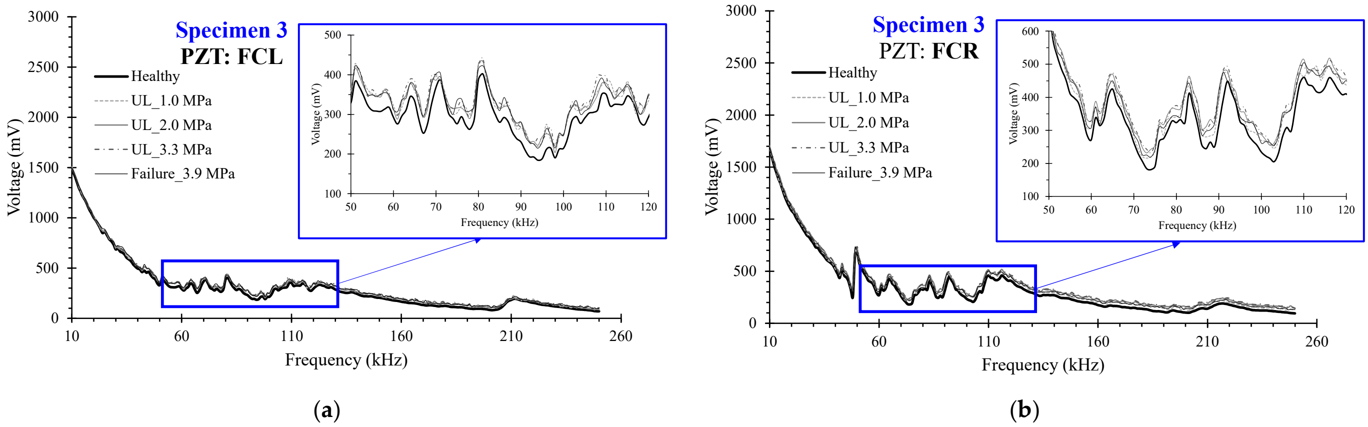

Figure 23. Typical voltage frequency response of the PZT (**a**) FCL and (**b**) FCR bonded to Specimen 3 under repeated flexural loading.

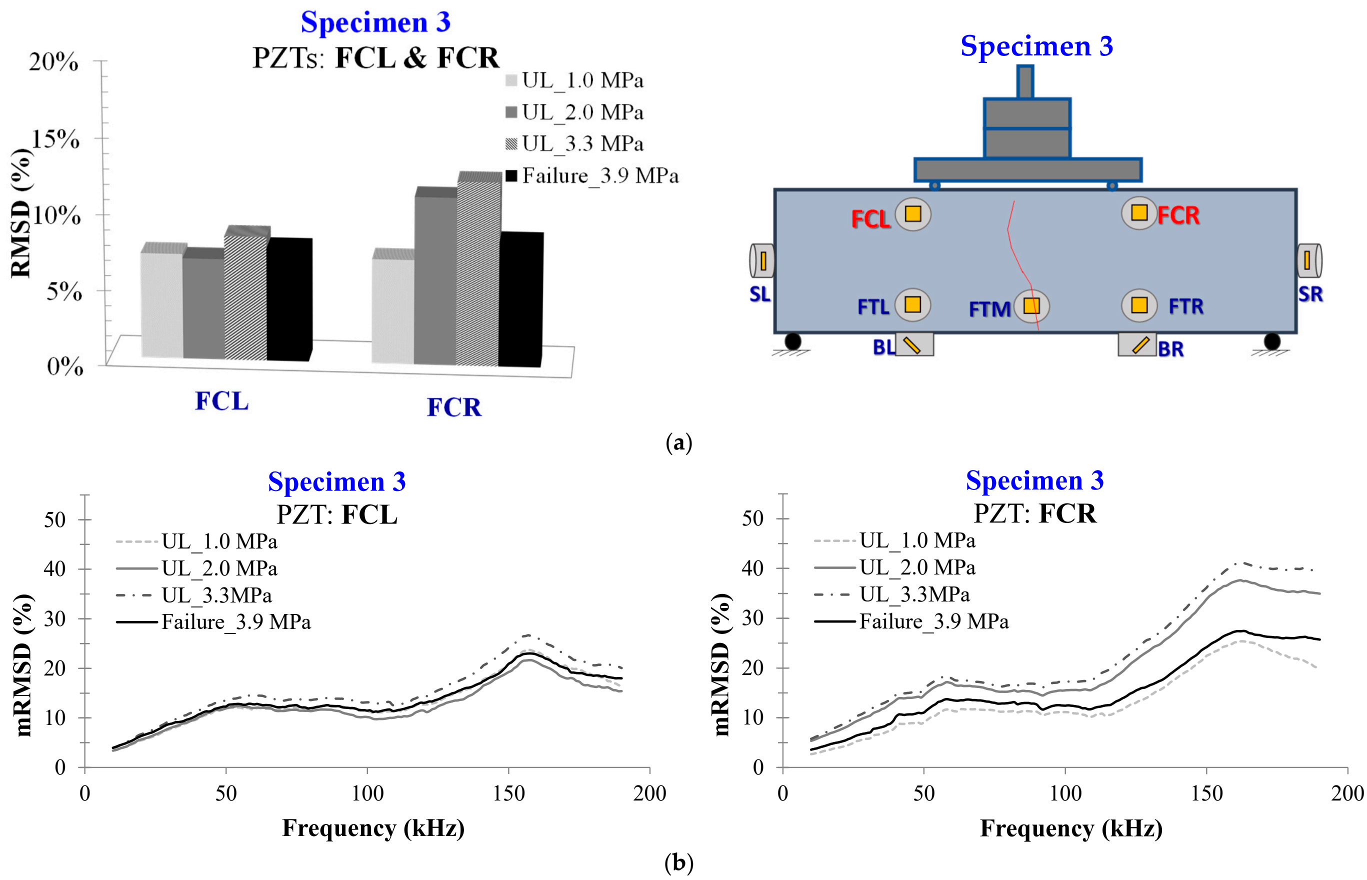

Figure 24. Damage assessment measurements in terms of (**a**) RMSD index ratio and (**b**) mRMSD index ratio of the PZT FCL and FCR bonded to Specimen 3.

PZTs FTR, FTM, and FTL were positioned in the tensile zone on the mid-span's right, middle, and left sections. These PZTs shared a parallel polarization direction with the forthcoming failure. However, PZT FTM was damaged during testing and was confirmed to have failed after the UL_3.3MPa damage level. As a result, no voltage response was observed after UL_3.3MPa. The crack's propagation into the PTZ transducer's body caused this failure. In addition, the crack propagated through the adhesive to the coated PZT, and this caused the cut of the transducer. The voltage signatures from the three PZTs shown in Figure 25 exhibit similar discrepancies. As shown in Figure 26, PZT FTL consistently exhibited a slightly higher RMSD index value at each damage level, although it was not significantly different from the values recorded by FTR. Furthermore, FTL and FTR displayed a very similar response regarding mRMSD ratios, as demonstrated in Figure 26.

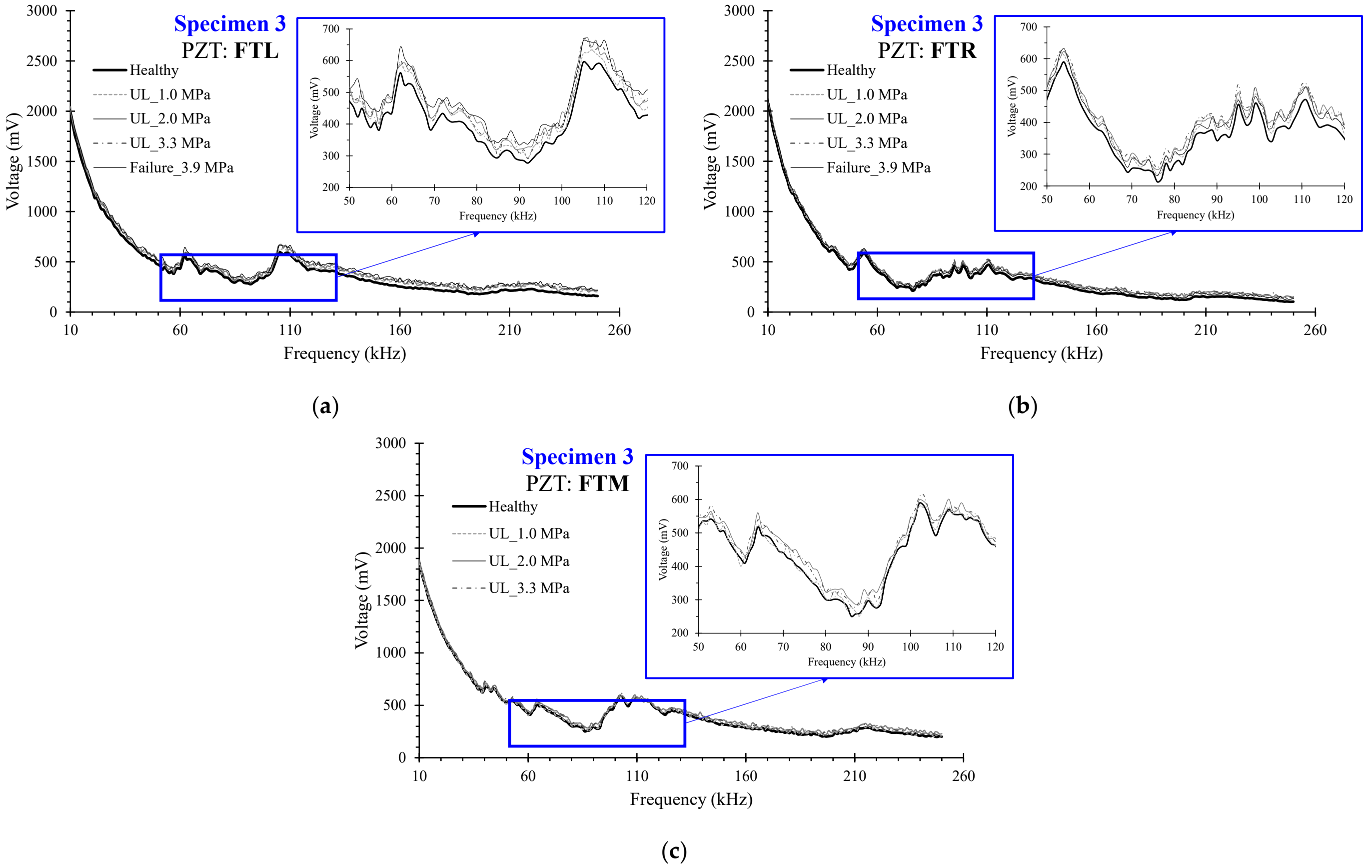

Figure 25. Typical voltage frequency response of the PZT (**a**) FTL, (**b**) FTR, and (**c**) FTM bonded to Specimen 3 under repeated flexural loading.

PZTs SR and SL were bonded to the outer sides, positioned in a vertical polarization direction to the impending failure. PZT SL was non-functional due to the electrode cut from the first voltage measurement. At the same time, PZT SR shows slight differences between damage levels, as depicted in Figure 27. However, although there is no comparison with the symmetric one of SL, the results for the SR PZT transducer showed an increased RMSD index value in the UL_3.3MPa damage level, considering that the failure formed at a distance of their limited monitoring capability. Figure 28 illustrates the RMSD and mRMSD plots for the PZT SR. All the trends of the PZT curves show the appearance of damage. The failure was shaped in the mid-span, and all the PZTs showed almost equal RMSD values and similar behavior to their relevant symmetric one. The fourth group cannot be evaluated due to the malfunction caused by PZT SL.

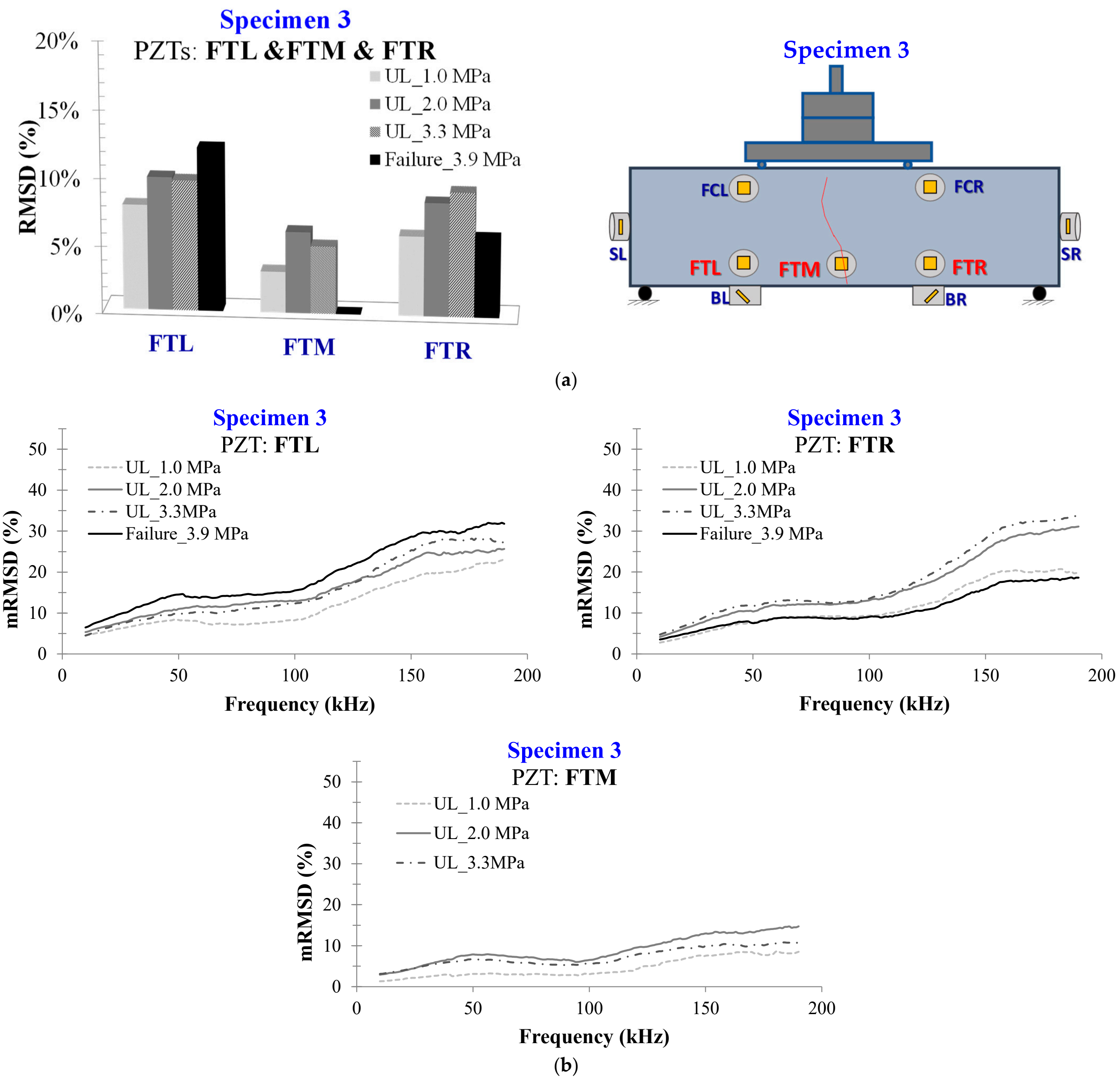

Figure 26. Damage assessment measurements in terms of (**a**) RMSD index ratio and (**b**) mRMSD index ratio of the PZT FTL, FTR, and FTM bonded to Specimen 3.

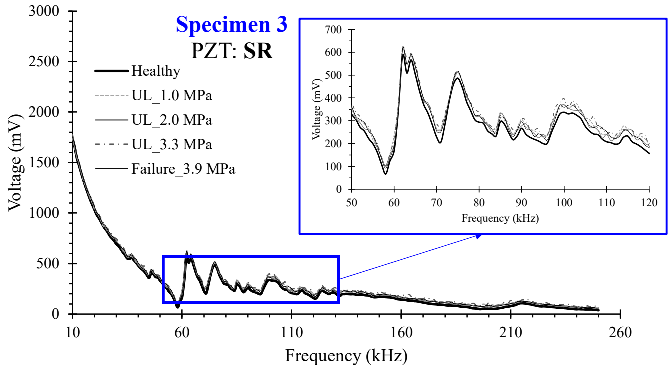

Figure 27. Typical voltage frequency response of the PZT SR bonded to Specimen 2 under repeated flexural loading.

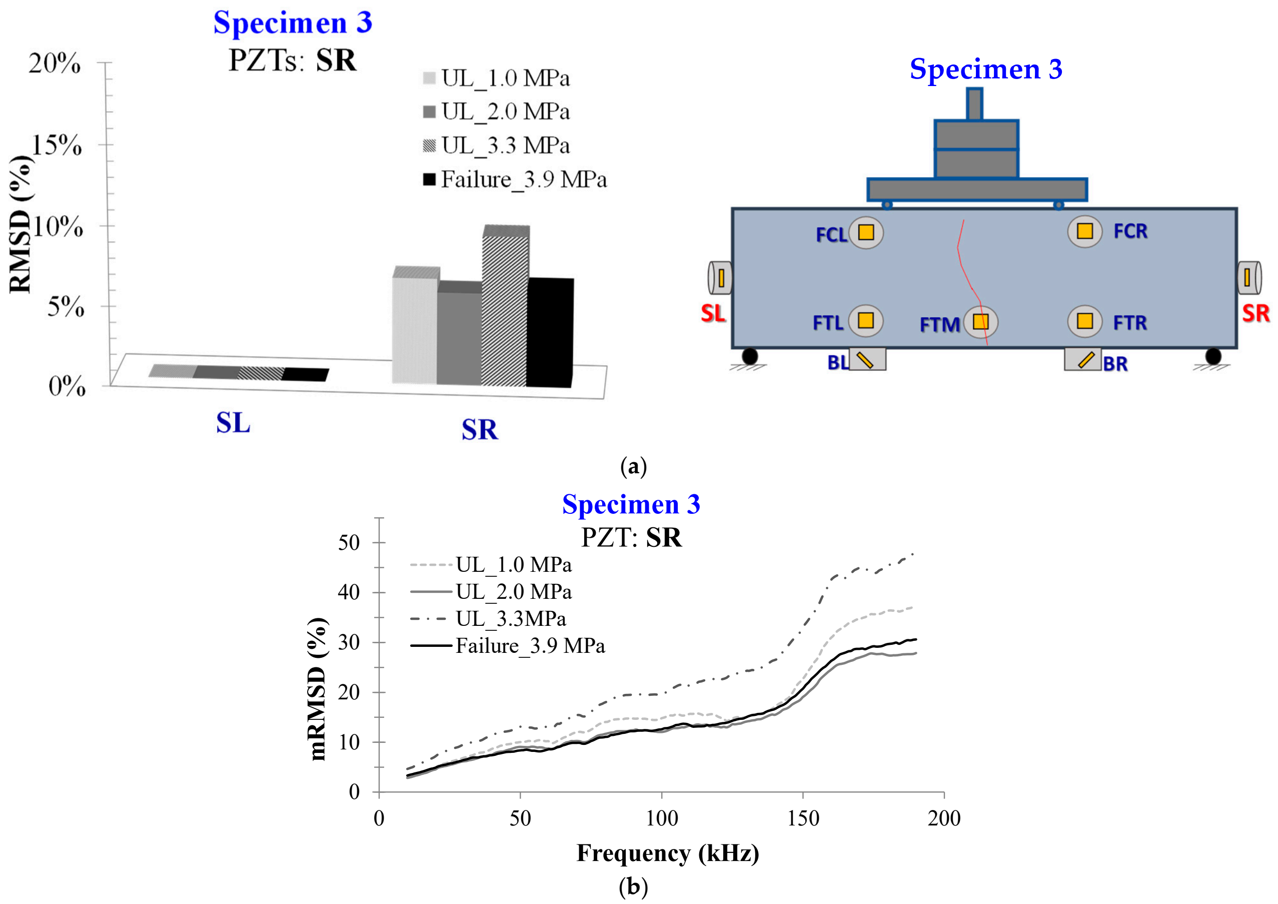

Figure 28. Damage assessment measurements in terms of (**a**) RMSD index ratio and (**b**) mRMSD index ratio of the PZT SL bonded to Specimen 3.

3.3. Discussion and Suggestions for Future Works

The diagnosis of damage due to cracking in the tested FRC specimens subjected to four-point bending repeated load has been achieved using a developed PZT-implemented EMI-based SHM system. Nevertheless, further investigation should be addressed in concrete structural members to overcome the following limitations.

Changes in the properties of the PZT's coat can cause variations in the voltage responses, causing potential false warnings. For this reason, the impact of these parameters should be eliminated through compensation algorithms by using multiple PZT transducers. Moreover, the EMI technique is a local method that uses high-frequency excitation. Thus, the sensing range is limited depending on the properties of the PZT sensor and the host structure dimensions. As such, cost issues could occur when monitoring large-scale structures since several PZT transducers are required to be employed. Thus, the effectiveness of the EMI-based SHM method in complex, real-life concrete structures should be checked and adequately established as an efficient real-time damage detection and continuous monitoring technique.

The initial step of the applied SHM technique is to acquire the reference frequency response (baseline signature) of each PZT transducer in the non-damaged state of the structural members. This reference signature is then compared to every damaged state at a later stage to identify any damage that occurred to the host structure. As it is virtually impossible to acquire an "absolutely healthy," or else a "no damage" state signature in existing real-life structures, future studies could be focused on creating an extensive database of measurements in multiple structural members, using several types of PZTs, under various loading conditions, to determine the current "reference" condition of the structure. Moreover, implementing an EMI-based SHM technique without using a reference signature, either by using the method alone or in combination with other NDT techniques [31], could be a challenging area of research.

4. Conclusions

This experimental study investigated the sensitivity of a PZT-enabled EMI-based system to identify and estimate early cracks in FRC specimens with synthetic fibers. The primary outcomes and findings of this study can be summarized as follows:

- Voltage frequency responses of the piezoelectric transducers extracted from the custom-made SHM system during the four-point testing measurements indicated significant discrepancies between the voltage signatures of the healthy and each examined damage levels for the three examined FRC specimens. These voltage changes mean the presence of potential cracks, and the increasing trend suggests the damage's severity;
- The well-known statistical index RMSD was successfully used to evaluate the cracking in FRC specimens while improving the efficiency and accuracy of damage detection;
- The new dynamic metric index, mRMSD, was successfully used to evaluate the cracking in FRC specimens while improving the efficiency and accuracy of damage detection;
- From the results obtained, an increasing upward trend in the values of the RMSD index results from the changes in the signal measurements of the PZTs, which confirm the damage's existence and the increase in the damage severity. Most of the above PZT signals exhibited such a response. Some fluctuations presented in the RMSD values are attributed to the shear lag effect [32] and the localized redistribution of the stresses in the specimens' internal mass through the transducer's effective monitoring area;
- The results suggest that the measurements obtained from PZT transducers installed to such specific locations or at a predefined angle created between the direction of the formed crack and the direction of the PZT's polarization could be useful in damage diagnosis and predict the forthcoming failure early damage stages, such as at the onset of the flexural crack;
- In the case of Specimen 2 and according to the previous conclusion, PZT mounted to the left side of the prism showed better results due to the angle of the crack formed, which is slightly inclined and towards the left span of the prism;
- The metric index mRMSD ensured the above aspect at most of the examined loading/damage levels;
- The effect of the PZT's coating to cause unwilling response variations and potential false warnings should be checked and limited through compensation algorithms. Further, the effectiveness of the proposed SHM technique in complex, large-scale, and real-life structures should be tested. Moreover, extensions and improvements of the EMI-based PZT-implemented monitoring techniques could be achieved by creating a database of measurements to determine the baseline structural condition or by combining this method with other NDT techniques.

Author Contributions: Conceptualization, M.C.N., C.E.C. and C.G.K.; methodology, M.C.N., C.E.C., A.I.K. and A.E.; validation, A.I.K. and A.E.; formal analysis, M.C.N., C.E.C. and C.G.K.; investigation, M.C.N.; data curation, M.C.N., A.I.K. and A.E.; writing—original draft preparation, M.C.N.; writing—review and editing, C.E.C. and C.G.K.; visualization, M.C.N. and A.E.; supervision, C.E.C., C.G.K. and A.I.K. All authors have read and agreed to the published version of the manuscript.

Funding: The authors also acknowledge support of this work by the project "Risk and Resilience Assessment Center—Prefecture of East Macedonia and Thrace-Greece". (MIS 5047293) which is implemented under the Action "Reinforcement of the Research and Innovation Infrastructure", funded by the Operational Programme "Competitiveness, Entrepreneurship and Innovation" (NSRF 2014–2020) and co-financed by Greece and the European Union (European Regional Development Fund).

Institutional Review Board Statement: Not applicable.

Data Availability Statement: The data presented in this study are available on request from the corresponding author.

Conflicts of Interest: The authors declare no conflict of interest.

References

1. Dong, W.; Li, W.; Tao, Z.; Wang, K. Piezoresistive Properties of Cement-Based Sensors: Review and Perspective. *Constr. Build. Mater.* **2019**, *203*, 146–163. [CrossRef]
2. Dong, W.; Li, W.; Lu, N.; Qu, F.; Vessalas, K.; Sheng, D. Piezoresistive Behaviours of Cement-Based Sensor with Carbon Black Subjected to Various Temperature and Water Content. *Compos. Part B Eng.* **2019**, *178*, 107488. [CrossRef]
3. Gribniak, V.; Kaklauskas, G.; Hung Kwan, A.K.; Bacinskas, D.; Ulbinas, D. Deriving Stress–Strain Relationships for Steel Fibre Concrete in Tension from Tests of Beams with Ordinary Reinforcement. *Eng. Struct.* **2012**, *42*, 387–395. [CrossRef]
4. Bencardino, F. Mechanical Parameters and Post-Cracking Behaviour of HPFRC According to Three-Point and Four-Point Bending Test. *Adv. Civ. Eng.* **2013**, *2013*, 179712. [CrossRef]
5. Bajpai, A.; Wetzel, B.; Klingler, A.; Friedrich, K. Mechanical Properties and Fracture Behavior of High-performance Epoxy Nanocomposites Modified with Block Polymer and Core–Shell Rubber Particles. *J. Appl. Polym. Sci.* **2020**, *137*, 48471. [CrossRef]
6. Vougioukas, E.; Papadatou, M. A Model for the Prediction of the Tensile Strength of Fiber-Reinforced Concrete Members, Before and After Cracking. *Fibers* **2017**, *5*, 27. [CrossRef]
7. Chalioris, C.E.; Panagiotopoulos, T.A. Flexural Analysis of Steel Fibre-Reinforced Concrete Members. *Comput. Concr.* **2018**, *22*, 11–25. [CrossRef]
8. Smarzewski, P. Study of Toughness and Macro/Micro-Crack Development of Fibre-Reinforced Ultra-High Performance Concrete After Exposure to Elevated Temperature. *Materials* **2019**, *12*, 1210. [CrossRef]
9. Voutetaki, M.E.; Naoum, M.C.; Papadopoulos, N.A.; Sapidis, G.; Chalioris, C.E. Cracking Diagnosis in Fibre Reinforced Concrete Cubes and Cylinders with Synthetic Fibres Using a PZT-Based Health Monitoring System. *Sch. J. Eng. Technol.* **2021**, *9*, 140–151. [CrossRef]
10. Mobasher, B.; Dey, V.; Bauchmoyer, J.; Mehere, H.; Schaef, S. Reinforcing Efficiency of Micro and Macro Continuous Polypropylene Fibers in Cementitious Composites. *Appl. Sci.* **2019**, *9*, 2189. [CrossRef]
11. Sapidis, G.; Naoum, M.; Papadopoulos, N.; Voutetaki, M. Flexural Damage Evaluation in Fiber Reinforced Concrete Beams Using a PZT-Based Health Monitoring System. In *International RILEM Conference on Synergising Expertise towards Sustainability and Robustness of Cement-Based Materials and Concrete Structures*; Jędrzejewska, A., Kanavaris, F., Azenha, M., Benboudjema, F., Schlicke, D., Eds.; RILEM Bookseries; Springer Nature Switzerland: Cham, Germany, 2023; Volume 43, pp. 957–968. ISBN 978-3-031-33210-4.
12. Kotecha, P.; Abolmaali, A. Macro Synthetic Fibers as Reinforcement for Deep Beams with Discontinuity Regions: Experimental Investigation. *Eng. Struct.* **2019**, *200*, 109672. [CrossRef]
13. Roesler, J.R.; Altoubat, S.A.; Lange, D.A.; Rieder, K.-A.; Ulreich, G.R. Effect of Synthetic Fibers on Structural Behavior of Concrete Slabs-on-Ground. *ACI Mater. J.* **2006**, *103*, 3–10.
14. Rainieri, C.; Fabbrocino, G.; Cosenza, E. Integrated Seismic Early Warning and Structural Health Monitoring of Critical Civil Infrastructures in Seismically Prone Areas. *Struct. Health Monit.* **2011**, *10*, 291–308. [CrossRef]
15. Ali, A.H.; Mohamed, H.M.; Chalioris, C.E.; Deifalla, A. Evaluating the shear design equations of FRP-reinforced concrete beams without shear reinforcement. *Eng. Struct.* **2021**, *235*, 112017. [CrossRef]
16. Bhalla, S.; Yang, Y.W.; Xu, J.F.; Soh, C.K. Damage Quantification Using EMI Technique. In *Smart Materials in Structural Health Monitoring, Control and Biomechanics*; Advanced Topics in Science and Technology in China; Springer: Berlin/Heidelberg, Germany, 2012; pp. 129–186. ISBN 978-3-642-24462-9.
17. Mei, H.; Haider, M.; Joseph, R.; Migot, A.; Giurgiutiu, V. Recent Advances in Piezoelectric Wafer Active Sensors for Structural Health Monitoring Applications. *Sensors* **2019**, *19*, 383. [CrossRef] [PubMed]
18. Perera, R.; Torres, L.; Ruiz, A.; Barris, C.; Baena, M. An EMI-Based Clustering for Structural Health Monitoring of NSM FRP Strengthening Systems. *Sensors* **2019**, *19*, 3775. [CrossRef] [PubMed]
19. Huo, L.; Cheng, H.; Kong, Q.; Chen, X. Bond-Slip Monitoring of Concrete Structures Using Smart Sensors—A Review. *Sensors* **2019**, *19*, 1231. [CrossRef]
20. Zapris, A.G.; Naoum, M.C.; Kytinou, V.K.; Sapidis, G.M.; Chalioris, C.E. Fiber Reinforced Polymer Debonding Failure Identification Using Smart Materials in Strengthened T-Shaped Reinforced Concrete Beams. *Polymers* **2023**, *15*, 278. [CrossRef]
21. Papadopoulos, N.A.; Naoum, M.C.; Sapidis, G.M.; Chalioris, C.E. Cracking and Fiber Debonding Identification of Concrete Deep Beams Reinforced with C-FRP Ropes against Shear Using a Real-Time Monitoring System. *Polymers* **2023**, *15*, 473. [CrossRef]
22. Karayannis, C.G.; Golias, E.; Naoum, M.C.; Chalioris, C.E. Efficacy and Damage Diagnosis of Reinforced Concrete Columns and Joints Strengthened with FRP Ropes Using Piezoelectric Transducers. *Sensors* **2022**, *22*, 8294. [CrossRef]
23. Chalioris, C.E.; Voutetaki, M.E.; Liolios, A.A. Structural Health Monitoring of Seismically Vulnerable RC Frames under Lateral Cyclic Loading. *Earthq. Struct.* **2020**, *19*, 29–44. [CrossRef]
24. Voutetaki, M.E.; Naoum, M.C.; Papadopoulos, N.A.; Chalioris, C.E. Cracking Diagnosis in Fiber-Reinforced Concrete with Synthetic Fibers Using Piezoelectric Transducers. *Fibers* **2022**, *10*, 5. [CrossRef]
25. Naoum, M.C.; Sapidis, G.M.; Papadopoulos, N.A.; Voutetaki, M.E. An Electromechanical Impedance-Based Application of Realtime Monitoring for the Load-Induced Flexural Stress and Damage in Fiber-Reinforced Concrete. *Fibers* **2023**, *11*, 34. [CrossRef]

26. *ASTM C 78–94*; Standard Test Method for Flexural Strength of Concrete (Using Simple Beam with Third-Point Loading). ASTM: West Conshohocken, PA, USA, 2002.
27. Naoum, M.C.; Sapidis, G.; Papadopoulos, N.A.; Chalioris, C.E. Damage Detection in Fiber Reinforced Concrete Specimens through the Application of a Novel Structural Health Monitoring System. In *The Challenges of Disaster Planning, Management, and Resilience*, 1st ed.; Chalaris, M., Ed.; Nova Science Publishers Inc.: Hauppauge, NY, USA, 2023; pp. 101–121.
28. Providakis, C.P.; Voutetaki, M.E. Electromechanical admittance—Based damage identification using Box-Behnken design of experiments. *SDHM Struct. Durab. Health Monit.* **2007**, *3*, 211–227. [CrossRef]
29. Providakis, C.P.; Liarakos, E.V. Web-Based Concrete Strengthening Monitoring Using an Innovative Electromechanical Impedance Telemetric System and Extreme Values Statistics: Web-Based Concrete Strengthening Monitoring System Using Impedance. *Struct. Control. Health Monit.* **2014**, *21*, 1252–1268. [CrossRef]
30. Parpe, A.; Saravanan, T.J. Surface-Mounted Smart PZT Sensors for Monitoring Damage Using EMI-Based Multi-Sensing Technique. In Proceedings of the 8th International Electronic Conference on Sensors and Applications, Virtual, 1–15 November 2021; p. 51.
31. Na, W.; Baek, J. A Review of the Piezoelectric Electromechanical Impedance Based Structural Health Monitoring Technique for Engineering Structures. *Sensors* **2018**, *18*, 1307. [CrossRef] [PubMed]
32. Bhalla, S.; Moharana, S. A Refined Shear Lag Model for Adhesively Bonded Piezo-Impedance Transducers. *J. Intell. Mater. Syst. Struct.* **2013**, *24*, 33–48. [CrossRef]